

HIGHWAY RESEARCH RECORD

Number 306

Geometric Design;
Protective Barrier Systems;
Luminaire Supports

6 Reports

Subject Areas

22 Highway Design
51 Highway Safety

HIGHWAY RESEARCH BOARD

DIVISION OF ENGINEERING NATIONAL RESEARCH COUNCIL
NATIONAL ACADEMY OF SCIENCES—NATIONAL ACADEMY OF ENGINEERING

WASHINGTON, D.C.

1970

Standard Book Number 309-01804-8

Price: \$2.20

Available from

Highway Research Board
National Academy of Sciences
2101 Constitution Avenue
Washington, D.C. 20418

Department of Design

W. B. Drake, Chairman
Kentucky Department of Highways, Lexington

L. F. Spaine
Highway Research Board Staff

GENERAL DESIGN DIVISION

M. D. Shelby, Chairman
Texas Transportation Institute, College Station

COMMITTEE ON GEOMETRIC HIGHWAY DESIGN (As of December 31, 1969)

W. A. Wilson, Jr., Chairman
North Carolina State Highway Commission, Raleigh

William P. Walker, Secretary
Bureau of Public Roads, Washington, D.C.

John E. Baerwald
Frederick G. Chatfield
P. B. Coldiron
W. A. Frick
Maynard Glass
C. William Gray
Peter J. Hunt

Nelson C. Jones
Jack E. Leisch
Robert L. Lewis
D. W. Loutzenheiser
J. Robert Moore
Val G. Rinehart

B. H. Rottinghaus
Bradford G. Sears
M. D. Shelby
Bob L. Smith
K. A. Stonex
John Walter

COMMITTEE ON GUARDRAIL, MEDIAN BARRIERS AND SIGN, SIGNAL AND LIGHTING SUPPORTS

(As of December 31, 1969)

Paul C. Skeels, Chairman
General Motors Proving Ground, Milford, Michigan

W. C. Anderson
John L. Beaton
Alan E. Brickman
Edward M. Conover
James J. Crowley
Albert L. Godfrey, Sr.
Malcolm D. Graham
Wayne Henneberger
Robert N. Hunter

John W. Hutchinson
Jack E. Leisch
J. E. McCracken
Eric F. Nordlin
Walter C. Oram
John M. Quigg
Edmund R. Ricker
Neilon J. Rowan

Frank G. Schlosser
J. Robert Stemler
Flory J. Tamanini
James A. Thompson
M. A. Warnes
Howard L. White
Earl C. Williams, Jr.
Robert Winans

Foreword

The highway design engineer is concerned with that phase of engineering dealing with the visible dimensions and features of the total highway. These design features are dictated by the requirements of traffic, site conditions, and economic considerations and must consider, among other things, vertical and horizontal alignment, cross section components, and safety devices and protective systems. The six papers included in this RECORD will be of considerable value to the design engineer in his decision-making processes.

The first paper offers a method to determine the optimum vertical highway alignment under specific conditions. Hayman presents a computer-oriented mathematical procedure capable of generating a sequence of feasible design statements. Design constraints and a general cost function are mathematically described in terms of alignment design variables.

Neuzil and Peet analyze the decision-making process involved in choosing between guardrail and flattened slopes on highway embankments. Economic break-even heights are determined by comparing construction and maintenance costs of embankments with costs of guardrail installation. In addition, safety break-even heights are determined by comparing the relative severity of accidents involving unprotected slideslopes with those involving collision with guardrails. Curves are presented that permit quick approximate study for proper selection of roadside treatment.

A 3-year program is being conducted to determine the feasibility of transferring unused National Aeronautics and Space Administration patents to the public sector. Kaplan, Hensen, and Fay report on the development of energy-attenuation systems for highway gores from NASA energy-absorbing devices. A method for the initial screening of available devices is presented and the evaluation of the remaining devices is discussed. Using scale-modeling techniques, procedures are developed for inexpensive and flexible testing of attenuation systems.

Hazardous locations such as the median opening between highway bridges require positive vehicle arresting systems in order to reduce the likelihood of severe accidents. Hayes, Hirsch, and Ivey report the results of full-scale testing of the "dagnet" arresting system consisting of a steel net anchored at each end to metal tape energy-absorbing devices. The entrapped vehicle is decelerated through resistance to reverse bending of metal tapes drawn between steel rollers. Decelerations encountered during the tests were significantly lower than those produced by rigid barriers. The authors present theoretical analyses that permit reasonably accurate predictions of vehicle stopping distance and deceleration levels.

One of the latest devices under development for protecting motorists from collisions with rigid roadside objects is a cellular crash cushion composed of lightweight, low-strength, vermiculite concrete. Results of three full-scale head-on crash tests led Ivey, Buth, and Hirsch to conclude that the cellular cushion is extremely effective in decelerating a vehicle within tolerable limits of restrained humans. Suggestions are made for construction and repair of the units in both in-place and precast configurations.

Martinez, Hirsch, Baskurt, and Jumper present the results of the mathematical simulation of vehicle collisions with single and dual support aluminum roadside sign structures mounted on frangible bases. The study was performed with a mathematical model and verified by full-scale crash tests using Maine sign and sign support configurations. Some important conclusions are given with regard to secondary collisions between the support and vehicle.

Contents

OPTIMIZATION OF VERTICAL ALIGNMENT FOR HIGHWAYS THROUGH MATHEMATICAL PROGRAMMING Robert W. Hayman	1
FLAT EMBANKMENT SLOPE VERSUS GUARDRAIL: COMPARATIVE ECONOMY AND SAFETY Dennis Neuzil and James S. Peet	10
SPACE TECHNOLOGY FOR AUTO-HIGHWAY SAFETY M. A. Kaplan, R. J. Hensen, and R. J. Fay	25
DRAGNET VEHICLE ARRESTING SYSTEM Gordon G. Hayes, T. J. Hirsch, and Don L. Ivey	39
FEASIBILITY OF LIGHTWEIGHT CELLULAR CONCRETE FOR VEHICLE CRASH CUSHIONS Don L. Ivey, Eugene Buth, and T. J. Hirsch	50
EFFECT OF VEHICLE COLLISION WITH ALUMINUM ROADSIDE SIGN STRUCTURES MOUNTED ON FRANGIBLE BASES J. E. Martinez, T. J. Hirsch, Yuce Baskurt, and J. J. Jumper	58

Optimization of Vertical Alignment for Highways Through Mathematical Programming

ROBERT W. HAYMAN, Department of Civil Engineering, Colorado State University

The design of the vertical alignment portion of a modern highway is an engineering problem of large computational magnitude characteristically possessing an unlimited number of solutions. In this paper, the familiar alignment problem is subjected to formal mathematical decision theory. An algorithm is developed that is capable of generating a sequence of feasible design statements and that terminates with an optimal design. The design algorithm is developed for rapid solution on a digital computer to produce a highly refined design statement. A list of design constraints is compiled and mathematically described in terms of the alignment design variables. A general cost function is derived in terms of the design variables. The design variables defined in the solution process are the centerline elevations and the location of the catch points at either side of the roadway.

•THE HIGHWAY design process is a recursive activity in which several separate phases are executed sequentially with the results of one phase establishing design considerations for the next. It would be desirable if even a single phase of this process could be executed to its optimal condition. This paper offers a method whereby one important design phase—that of vertical alignment—may be executed to its optimal condition.

It is not to be implied that all considerations of the problem are complete. The intent is to establish the nature of the design methodology and to be only inclusive enough to demonstrate the promise of the technique.

It is presumed that a statement of horizontal alignment is available as a starting point and that a refined statement of the vertical alignment is desired. The optimal vertical alignment is effected through the application of mathematical programming.

PROBLEM STATEMENT

The requirement of casting a problem into a form that may be solved by the general application of mathematical programming theory is that specifications and value judgments that describe some feature of the design or will constrain its final form are subject to quantification. In addition, one must have a clear objective in mind for the final design—that is, some statement representing that quality or group of qualities against which various designs may be compared, thus permitting rejection of all feasible solutions except the optimal. Such a statement of objectives must also be subject to quantification. This statement is known as the objective function. For example, the design objective could be to achieve the smallest initial construction cost, or to provide a facility having the likelihood of the smallest maintenance cost or smallest accident hazard, or maximum traffic capacity, to name only a few of the more popular criteria. The condition selected for this demonstration is that of smallest initial construction cost.

The general form of any mathematical programming problem is as follows:

Given a set of design variables

$$X_1, X_2, X_3, \dots, X_n$$

and a set of design specifications

$$\left. \begin{array}{l} g_1 (X_1, X_2, X_3, \dots, X_n) \leq b_1 \\ g_2 (X_1, X_2, X_3, \dots, X_n) \leq b_2 \\ \cdot \\ \cdot \\ g_m (X_1, X_2, X_3, \dots, X_n) \leq b_m \end{array} \right\} \text{Constraints}$$

and a design objective

$$Z = f(X_1, X_2, X_3, \dots, X_n)$$

find values for $X_1, X_2, X_3, \dots, X_n$ that satisfy all constraints and result in the minimum value of the design objective.

Currently there exist several techniques that will directly generate a set of values for the design variables in such a manner that all design constraints are satisfied. Beginning with some initial, feasible solution, any one of the various mathematical programming algorithms will seek out a new feasible solution that shows an improvement in the design objective when compared to the first solution. The programming algorithm will contain some mechanism for perpetuating the recursion process that will continue until no new solution can be found that will improve the design objective. In some cases it is even possible to say with absolute certainty that no better solution actually exists.

The particular solution methodology thought to be best suited for solving the vertical alignment problem will be discussed in a later section. At this point, the task at hand is one of development of the design constraints.

MATHEMATICAL MODELS FOR DESIGN CONSTRAINTS

A single list of design constraints for the vertical portion of the highway system could not hope to represent the needs of any particular design agency and are not intended to do so. A selected list of design constraints is as follows:

1. Maximum roadway grade limitations are not to be exceeded;
2. Parabolic (second order) curves shall be used as necessary to provide for changes in direction of the vertical attitude of the centerline;
3. The profile is to provide for continuous minimum safe line-of-sight distances;
4. The vertical accelerations of vehicles traveling at designed speed are to be held to comfortable minimums;
5. Limitations on the stability of cut and fill slopes must be accounted for, presuming knowledge of suitable soil strength parameters;
6. Provision must be made to recognize that the roadway elevation and/or catch point location may be prespecified according to some existing physical condition; and
7. Earthwork quantities are to be balanced considering the possibility of wasting excess excavation and borrowing to account for any deficiency in required fill volumes.

Numerical values applying to the interpretation of some constraints can be taken from "A Policy on Geometric Design of Rural Highways" (1), a publication of the American Association of State Highway Officials, or from other relevant specifications.

The design variables selected for identification are the roadway elevations on the centerline of the roadway and, at each design station, the lateral location of side-slope catch points. Thus, at a given design station along the centerline of the roadway, three variables must be identified.

The symbology for modeling the problem is set down at the outset as follows:

- j = the parameter for numbering the design stations;
- X_j = the centerline elevation at station j ;
- $X_{j,1}$ = the distance measured laterally from shoulder or ditch point to the right-hand catch point;
- $X_{j,2}$ = the distance measured laterally from shoulder or ditch point to the left-hand catch point;
- E_j = elevation of natural ground on the centerline at station j , presumed known;
- $2K^f$ = width of roadway in a fill section, presumed known;
- $2K^c$ = width of roadway in a cut section, presumed known;
- L = horizontal distance interval between adjacent design stations, a fixed quantity;
- G = tangent grade;
- β_j = "average" slope of the natural ground line for the cross section at station j ;
- n = number of design stations on some particular project;
- $S_{j,1}$ = cut or fill slope on the right-hand side of the template at station j ; and
- $S_{j,2}$ = cut or fill slope on the left-hand side of the template at station j .

Much of the mathematical detail required for development of the constraint modeling is not included here. A complete discussion may be found elsewhere (2). Figures 1 and 2 will offer some assistance in the interpretation of the constraint forms given below.

1. Grade Restriction—Call G_{\max} the absolute value of the limiting centerline grade, between any two consecutive stations. Then

and

$$\left. \begin{array}{l} X_{j+1} - X_j \leq G_{\max} L \\ X_j - X_{j+1} \leq G_{\max} L \end{array} \right\} j = 1, 2, \dots, n - 1 \quad (1)$$

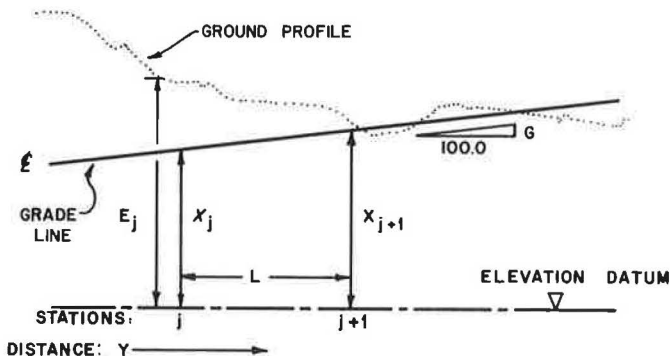


Figure 1. Hypothetical roadway profile.

5. Preset Values or Tolerances on Design Variables—Suppose, at roadway station j , that the centerline elevation were required to be 5000.00 ft, plus or minus 0.10 ft. Then

$$\text{and} \quad \left. \begin{array}{l} X_j \leq 5000.10 \\ X_j \geq 4999.90 \end{array} \right\} \text{any } j \quad (4)$$

is required. Any such statement may be incorporated into the model, as may be required.

6. Slope Stability Constraint—It is presumed that side-slope limitations are known for any design station. Call these $S_{j,1}$ and $S_{j,2}$ for the right- and left-hand slopes respectively. In Figure 2 a typical cut section is shown. In this representation, the natural ground line has been replaced by a single best-fit line. Statistical techniques have been successfully used (2) as a practical method for describing the attitude of the best-fit line. In terms of the idealized template, the slope protection may be provided by the following collection of statements:

$$-X_j \left(\frac{S_{j,1}}{1 - \beta_j S_{j,1}} \right) - X_{j,1} \leq \left(\frac{S_{j,1}}{1 - \beta_j S_{j,1}} \right) (E_j + \beta_j K^c) \quad (5)$$

for a right-hand cut slope, and

$$X_j \left(\frac{S_{j,1}}{1 + \beta_j S_{j,2}} \right) - X_{j,2} \leq \left(\frac{S_{j,2}}{1 + \beta_j S_{j,2}} \right) (E_j - \beta_j K^c) \quad (6)$$

for a left-hand cut slope, and

$$X_j \left(\frac{S_{j,1}}{1 + \beta_j S_{j,1}} \right) - X_{j,1} \leq \left(\frac{S_{j,1}}{1 + \beta_j S_{j,1}} \right) (E_j + \beta_j K^f) \quad (7)$$

for a right-hand fill slope, and

$$-X_j \left(\frac{S_{j,2}}{1 - \beta_j S_{j,2}} \right) - X_{j,2} \leq \left(\frac{S_{j,2}}{1 - \beta_j S_{j,2}} \right) (E_j - \beta_j K^f) \quad (8)$$

for a left-hand fill slope.

Only two of constraints 5 through 8 are required at any particular design station. To make a proper choice, it is required that a preliminary vertical alignment be roughed out. An inappropriate initial choice of pairs of stability constraints has been found to have very little effect on the final solution (2).

7. Material Balance Constraint—The total of that material to be excavated plus any borrow must be at least as great as the total embankment plus any waste. In a gross mathematical way this says

$$V^c + B \geq V^f + W$$

or

$$V^c - V^f + B - W \geq 0$$

where V^c , B , V^f , W are respectively total excavation, total borrow, total fill, and total waste. It remains to reconstruct this relationship in terms of the design variables.

The fundamental unit to be considered is the cross-sectional area of the roadway template at any design station. Figure 2 serves to represent the discussion. Recall that the actual cross-profile of the ground line has been replaced by a statistically fit line. The attitude of this line is β , and is known. For a typical cut section, the template area may be expressed as

$$A_j = -2K^c X_j + 2K^c E_j + \frac{1}{2} (E_j - X_j + \beta_j K^c) X_{j,1} + \frac{1}{2} (E_j - X_j - \beta_j K^c) X_{j,2} \quad (9)$$

For a typical fill section, at station j,

$$A_j = 2K^f - 2K^f E_j + \frac{1}{2} (E_j + X_j - \beta_j K^f) X_{j,1} + \frac{1}{2} (-E_j - X_j - \beta_j K^c) X_{j,2} \quad (10)$$

All elements in definitions 9 and 10 are known except the design variables X_j , $X_{j,1}$, and $X_{j,2}$. Assuming for the moment that we know which stations in the project are cut and which are fill, the gross form of the material balance constraint may be specialized:

$$\frac{L}{54} \sum_j^{\text{cuts}} (A_j + A_{j+1}) - \frac{L}{54} \sum_j^{\text{fills}} (A_j + A_{j+1}) + B - W \geq 0 \quad (11)$$

Substitution of definitions 9 and 10 into the specialized form, 11, produces the final working form of the material balance requirement. Lack of space and of a specific example precludes this last act. Actually, an electronic computer makes very short work of the process.

It must be supposed that there will be initial error in constructing the material balance constraint, as the final design is not known at this point. Accordingly, there will have been incorrect identifications of which sections are cut and which are fill. However, since the solution process is itself recursive in nature, corrections to the cut/fill designations may be made during the actual solution process. Experience to date (2) indicates that the entire procedure stabilizes quite rapidly.

The final modeling problem concerns the construction of the design objective function. Details of development are similar to those involved in formulating the material balance statement.

DESIGN OBJECTIVE FUNCTION

Recall that the design objective is to determine the solution for the design variables that results in a minimum construction cost. The objective function is developed as follows:

Define

U^c = unit of cost of excavation,

U^f = unit cost of fill,

U^b = unit cost of borrow (delivered),

U^w = unit cost of waste (cost above excavation), and

U^h = unit cost of haul from cut to fill (cost/station-yard).

Recall that

$$V^c = \text{volume of excavation} = \frac{L}{54} \sum_j^{\text{cuts}} (A_j + A_{j+1})$$

$$V^f = \text{volume of fill} = \frac{L}{54} \sum_j^{\text{fill}} (A_j + A_{j+1})$$

In addition, let

$$V_j = \text{volume of excavation between station } j \text{ and } j + 1 = \frac{L}{54} (A_j + A_{j+1})$$

H_j = distance of hauling V_j to an appropriate fill zone

Now let C^c , C^f , C^h , C^b represent the total costs of excavation, fill, haul, and borrow respectively. It is assumed that waste costs nothing beyond excavation costs. Then, the total project cost can be stated as follows:

$$\begin{aligned} C &= C^c + C^f + C^h + C^b \\ &= \frac{U^c L}{54} \sum_j^{\text{cuts}} (A_j + A_{j+1}) + \frac{U^f L}{54} \sum_j^{\text{fill}} (A_j + A_{j+1}) \\ &\quad + \frac{U^h L}{54} \sum_j^{\text{cuts}} (A_j + A_{j+1}) H_j + U^b B \end{aligned} \quad (12)$$

On the basis of some starting statement for the vertical design, the objective function 12 is specialized for any given project by the substitution of the template area definitions, Eqs. 9 and 10, and estimation of the H_j . It is recognized that there are other construction costs than those accounted for by Eq. 12. However, the major ones are relatively constant over a wide range of possible vertical alignments. Accounting for these costs, therefore, contributes nothing to a solution for the design variables being considered. Further, accounting for fill costs in the manner described is contrary to standard highway accounting procedures. It must be recognized, however, that there are real costs associated with embankment construction. Watering or dewatering, compaction, and shaping are examples of these. The only question in accounting for fill costs on a cubic yard basis is the accounting method.

SOLUTION PROCESS

The selection of a particular solution procedure must consider various characteristics of the mathematical programming problem. Of importance are size of the problem, mathematical nature of the inequalities and objective function, and whether or not an approximate solution is acceptable. The procedure selected will produce an "exact" solution, at least theoretically, and is thought to require a minimum amount of computational effort.

Consider the following computational sequence:

1. Somehow, define a starting solution, $\bar{X}^0 = (X_1^0, X_2^0, \dots, X_n^0)$.
2. Compute the gradient of the objective function and evaluate this at

$$\bar{X}^0; \bar{\nabla} f(\bar{X}^0) = \left[\frac{\partial f}{\partial X_1}(\bar{X}^0), \frac{\partial f}{\partial X_2}(\bar{X}^0), \dots, \frac{\partial f}{\partial X_n}(\bar{X}^0) \right]$$

For convenience, let \bar{d}^0 equal the transpose of $\bar{\nabla} f(\bar{X}^0)$.

3. Form the relation $\bar{X}^1 = \bar{X}^0 + \lambda \bar{d}^0$, where λ is some non-negative scalar constant.
4. The relationship defined in 3 may be substituted into each constraint, treated as an equality. The resulting statements may each be solved for λ . Identify the smallest $\lambda = \lambda_{\min}$.

5. $\bar{X}^1 = \bar{X}^0 + \lambda_{\min} \bar{d}$. Now \bar{X}^1 is a better solution than \bar{X}^0 and is a feasible solution.

6. Repeat steps 2 through 5 until no non-zero λ can be calculated at step 4. When this occurs, the computational sequence must be altered, as discussed later.

The process offered below is called the "method of feasible directions" and was developed by Zoutendijk. The details are thoroughly discussed elsewhere (2, 3, 4). Suppose that the cyclic process described above terminates at cycle V. We are looking for a new solution which is better than \bar{X}^V and is still feasible.

7. Form the relationship

$$\bar{X}^{V+1} = \bar{X}^V + \lambda \bar{r}$$

where $\bar{r} = (r_1, r_2, \dots, r_n)$. We seek to discover \bar{r} which, for any non-negative scalar λ , will produce a feasible \bar{X}^{V+1} that is better than \bar{X}^V .

8. Solve the following mathematical programming problem.

$$\bar{\nabla} g_i(\bar{X}^V) \bar{r} + \sigma \leq 0 \quad (i \text{ contained in } I_V)$$

$$-f(\bar{X}^V) \bar{r} + \sigma \leq 0$$

$$r_1^2 + r_2^2 + \dots + r_n^2 = 1$$

Maximize σ .

In the programming problem given above the new terminology is identified as follows:

$$\bar{\nabla} g_i(\bar{X}^V) = \left[\frac{\partial g_i}{\partial X_1}(\bar{X}^V), \frac{\partial g_i}{\partial X_2}(\bar{X}^V), \dots, \frac{\partial g_i}{\partial X_n}(\bar{X}^V) \right]$$

I_V = that subset of the original constraints that became active (strict equalities) at cycle V.

σ = auxiliary variable, of no relationship to the original variables (and of no further interest beyond step 8).

Hadley (3) shows how this auxiliary programming problem can be further transformed into a completely linear problem. Having accomplished this, it may be solved by the well-known simplex algorithm. It is significant that the auxiliary problem is normally but a fraction of the size of the original problem.

9. With \bar{r} now known, substitute $\bar{X}^{V+1} = \bar{X}^V + \lambda \bar{r}$ into all constraints of the original problem, solving for λ in each case. Using the minimum λ , form

10. $\bar{X}^{V+1} = \bar{X}^V + \lambda_{\min} \bar{r}$. Now \bar{X}^{V+1} is better than \bar{X}^V , and is still feasible.

11. Repeat steps 8 through 10 until no non-zero λ may be found.

The entire process is at an end with the final solution point being either a relative (local) optimum or an absolute optimum.

CONCLUSION

In an application of these techniques to a portion of a highway project that had previously been designed by classical methods (2), the computed construction cost was reduced from \$106,000 per mile to \$86,000 per mile. All design constraints were satisfied and an entirely continuous curvilinear alignment was produced. To design a typical mile of roadway according to those constraints outlined in the discussion, it is necessary to write approximately 308 constraints like Eqs. 1 through 11 and there will

be approximately 160 design variables involved. A CDC 6400 computer system was used for the various computational phases and can effect a final solution (after data preparation) in about 10 minutes.

REFERENCES

1. A Policy on Geometric Design of Rural Highways. American Association of State Highway Officials, Washington, D. C., 1965.
2. Hayman, Robert W. Mathematical Programming Solution for Optimal Design of Vertical Alignment of Highways. University of Colorado, Boulder, PhD thesis, 1968.
3. Hadley, G. Nonlinear and Dynamic Programming. Addison-Wesley, Reading, Mass., 1964.
4. Zoutendijk, G. Methods of Feasible Directions. Elsevier Publishing Co., Amsterdam, Holland (D. Van Nostrand, Princeton, N. J., distributors), 1960.

Flat Embankment Slope Versus Guardrail: Comparative Economy and Safety

DENNIS NEUZIL and JAMES S. PEET, Department of Civil Engineering,
University of Delaware

The thesis that the aesthetically designed highway is usually the most economical highway to construct and maintain and is inherently safe is examined with respect to one important design component having substantial aesthetic significance: roadside design over embankments. The equal-cost or economic break-even height of embankment is determined for a range of unit construction and maintenance costs and basic types of embankment profiles. The relationship between economic break-even height and safety break-even height—the height at which an unprotected sideslope is equal in accident severity to collision with guardrail—is examined.

Economic break-even height varies considerably with unit costs and embankment profile and is generally well below the safety break-even height; thus there is a wide span in fill height over which guardrail installation is cheaper than slope flattening, but design with flattened slope is safer. Economic break-even heights for embankments of smoothly varying height are significantly greater than those for constant-height embankments. Right-of-way cost in rural areas is likely to have little effect on break-even height, while culvert cost can considerably reduce it. The results of this study together with what appears to be an excessive amount of roadside guardrail over embankments on rural highways and at interchanges indicate that many highway designers substantially underestimate the economic break-even height for flattened sideslopes.

•INCREASINGLY it is suggested that the aesthetically designed highway is often more economical than less attractive designs when all costs are fully considered and that the aesthetically pleasing highway is often the safest highway. This paper analyzes the range of validity of this thesis with respect to one important geometric design component having substantial aesthetic significance: the treatment of the "roadside system" over embankments, or more specifically, the use of flat fill slopes rather than steep slopes protected by guardrail.

The philosophy seems to persist among many highway designers that any design treatment that departs from minimum geometric standards in order to improve appearance is likely to increase highway cost substantially. This is especially evident in roadside design, where a predilection to minimize earthwork by utilizing steep sideslopes results in what appears to be an excessive amount of guardrail on even our newest high-type highways. At the same time, the relative safety of flattened slopes compared with guardrail is apparently not fully recognized.

The following sections present an analysis of the range of "economic break-even height"—the fill height at which flattened slope treatment and design with guardrail are equal in total annual cost—and examines the relationship between the economic break-even height and what might be called the "safety break-even height".

SELECTION OF ROADSIDE TREATMENT

The decision as to roadside treatment—guardrail or flat slope—should be based on three criteria: economy, safety, and aesthetics. The essential variables affecting economy and safety and their interrelationships are shown in Figure 1.

Economy

Embankment cost and guardrail cost are usually given primary consideration in choosing between the two alternate roadside designs. However, there are other construction costs, as well as maintenance costs, that merit consideration. The design of minimum construction cost is not always the design of minimum total annual cost to the highway agency when maintenance costs are properly included in economy studies.

Construction cost varies with embankment height and sideslope steepness, inasmuch as these two variables determine fill quantity, surface area requiring topsoil and seeding, the need for guardrail and its attendant installation cost, and the cost of culverts crossing beneath the embankment. High embankments with flat sideslopes may necessitate purchase of a considerable amount of additional right-of-way or slope easements. The cross slope of the original ground line will influence several of these costs.

Maintenance costs also vary with embankment height and slope steepness. Mowing cost is a function of slope surface area (dependent on embankment height and slope) and of slope steepness. Erosion problems tend to increase as slope steepness increases, and the surface area subjected to erosion is a function of slope and embankment height. Snow drifting and snow removal costs are influenced by slope steepness and also by the presence of guardrail. Finally, the guardrail itself requires maintenance such as painting and repair after severe collisions. Maintenance costs of course vary considerably with climatic conditions.

A third cost element, in addition to construction and maintenance costs, is the cost of accidents, which depends on the severity of the accident—collision with the guardrail or running off the roadway onto the sideslope—and the number of such accidents. Although accident costs are difficult to quantify, they should be included in the total econ-

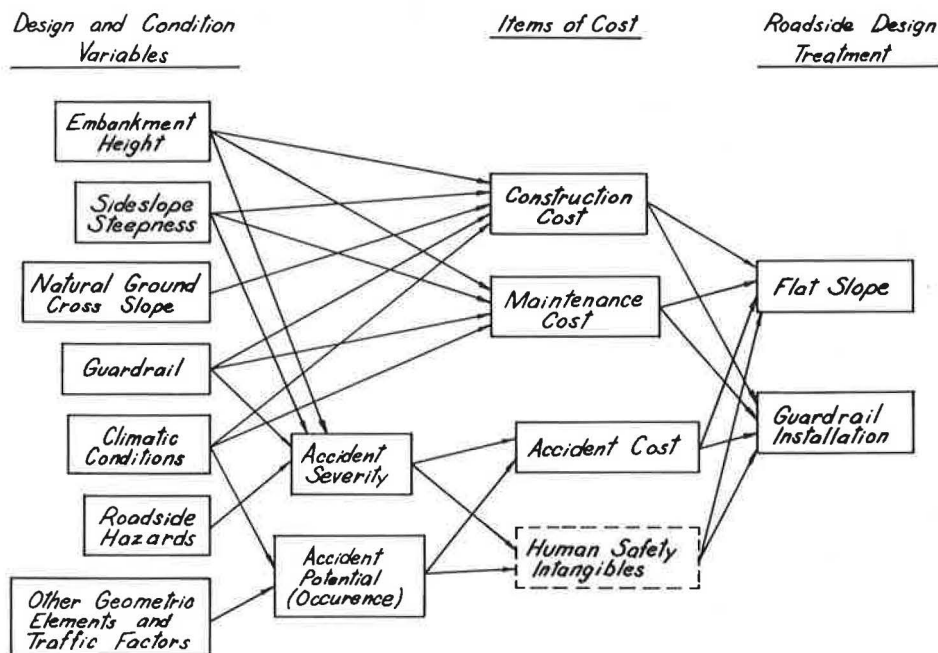


Figure 1. Economy and safety determinants of roadside design treatments.

omy study. An appraisal of ran-off-the-roadway probability at a particular location is helpful in itself, especially where economic analysis shows design with guardrail is cheaper but a flattened slope is less hazardous.

Safety

A vehicle that leaves the roadway is subject to an accident hazard that depends on the type of guardrail, or in the absence of guardrail, on the embankment height, slope steepness, and roadside obstacles. The probability that a vehicle will leave the roadway depends of course on many factors, such as geometric design elements, traffic conditions, and climate conditions.

The "equal severity index" concept developed by the California Division of Highways is perhaps the most valid approach to the question of the relative safety of flat slopes and guardrail (1, 2). Essentially, guardrail is warranted only if the severity of damage and injury from collision with guardrail is less than that sustained by traveling down the embankment slope. The equal severity curve for typical corrugated or W-beam guardrail is shown in Figure 9. Points along the curve define slope-height combinations for unprotected embankments that have severity equal to that for collision with guardrail. Thus, the shaded region above the curve represents slope-height combinations that warrant guardrail installation from a safety standpoint, while guardrail should not be installed for slope-height combinations below the curve unless there are severe roadside hazards close to the roadway, such as culvert endwalls, heavy signposts, or bodies of water at the toe of the slope.

Contrary to what might be expected, the California study found that the cross slope of the original ground at the toe of the embankment had no significant correlation with the severity of ran-off-the-roadway accidents (1).

Aesthetics

There can be little disagreement that guardrail diminishes the attractiveness of the highway. It is more than the man-made "hardware" appearance of the guardrail and the rusted, dented, paint-peeled areas along with kinks in alignment and ragged vegetation often seen under the guardrail that makes it so aesthetically unpleasing. It is also the visual discord that it creates: occurring intermittently along the highway, it produces a longitudinal discontinuity in the flow of the highway alignment. It not only starts and ends abruptly but also in some cases weaves from side to side. Guardrail also produces a discontinuity in the smooth flow of the highway cross section, chopping up the roadway "space" and interfering with the attainment of a smooth merge of highway with terrain, and often producing a feeling of confinement or lateral friction in the driver (especially with guardrail at both roadsides) compared to the open feeling that obtains without guardrail and with gentle fill slopes.

In addition, the steeper slopes usually used with guardrail installation are unnatural looking and therefore unattractive in all but the steepest terrain, and they are often eroded. Both of these features may be visible to the motorist under certain conditions of alignment and are often visible to those who abut the road (the "view of the road").

Of course, there are situations where steep fill slopes and attendant use of guardrail may be more desirable than flatter slopes from an aesthetic viewpoint, as in the case where it is desired to minimize clearing of wooded areas near the roadside or to minimize encroachment upon streams and lakes. However, here the best solution is often to be found in realignment or relocation of the highway.

Range of Outcomes for Economy and Safety Analyses

Although flat slopes are generally to be favored over guardrail design insofar as aesthetics are concerned, economy and safety may favor either roadside treatment. For any given flat slope compared to a steep slope with guardrail, four possible combinations of safety and economy may occur depending on embankment height and unit construction and maintenance costs. These are shown schematically in Figure 2.

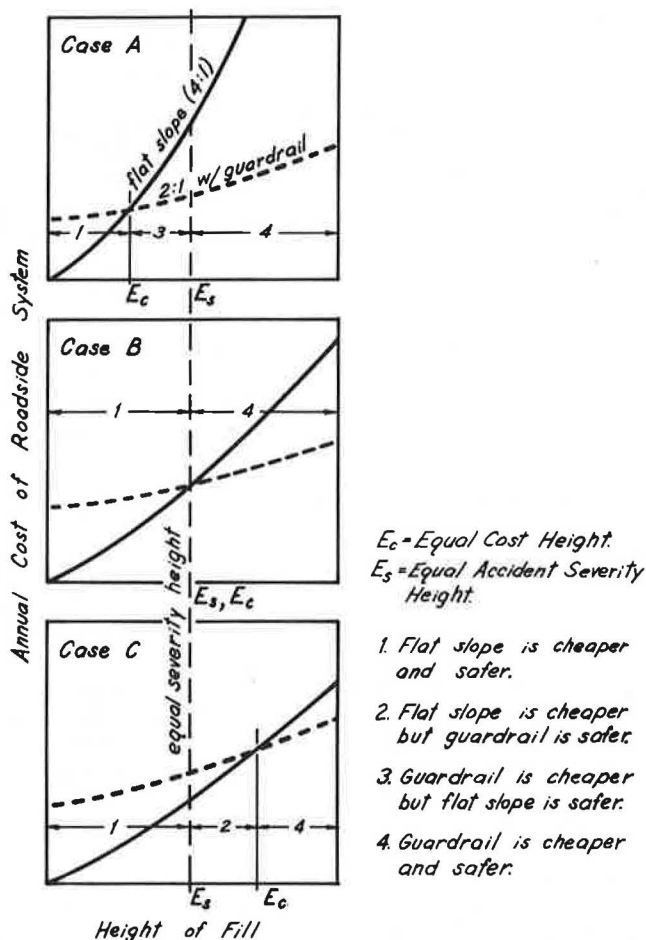


Figure 2. Relationship between economic and safety break-even heights for two alternative roadside treatments.

For the cost conditions of Case A, the economic break-even or equal-cost embankment height, E_c , lies to the left of the equal-safety height, E_s , as determined from the equal severity curve discussed earlier. Thus, for all embankment heights less than E_c , it is both cheaper and safer to use a flat slope without guardrail—a clear-cut decision for flat slope treatment. For heights between E_c and E_s guardrail is cheaper but flat slope design is safer. The designer must decide whether the greater safety of the flat slope design is worth the additional cost. If accident costs have not been included in the annual costs of the alternate roadside treatments, the consideration of overall accident potential at the site, as distinct from accident severity, may aid in the final selection of design treatments. Thus if the accident potential is low—short embankment length, good alignment light traffic, etc.—the designer may decide in favor of the guardrail design even though the flat slope design is safer. If the site conditions are such that accident potential is high, the cost of frequent and extensive guardrail repairs may make the flat slope treatment feasible from both economy and safety standpoints. There is a clear-cut decision for guardrail in terms of both safety and economy for embankment heights to the right of E_s .

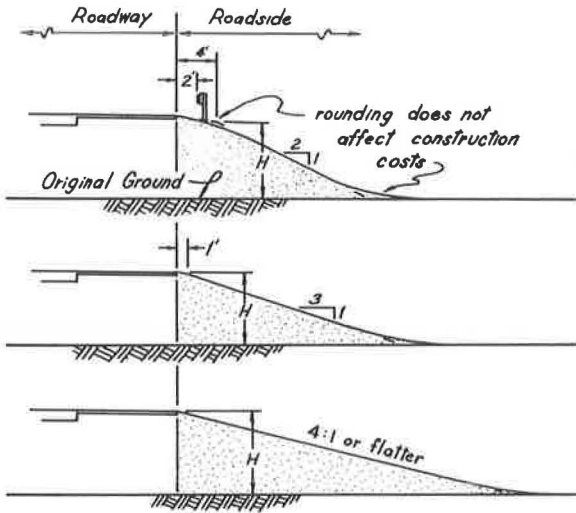


Figure 3. Alternative roadside treatments.

lying beyond the outer edge of the shoulder as shaded in Figure 3. The "standard" guardrail roadside design treatment with which the flatter slope treatments will be compared consists of a 2:1 sideslope combined with an additional 4-ft shoulder extension to provide room for secure installation of guardrail and to provide a "usable" shoulder that is equivalent, after rounding, to that available when sideslopes are 4:1 or flatter (3, 4). The additional cost due to this extra width is properly assignable to the guardrail design. The 3:1 slope design also requires widening in order to provide a fully usable shoulder.

In the following cost analyses the unit cost of fill has been applied to the theoretical earthwork volumes, but shrinkage or swell can be assumed to be accounted for in the unit fill cost itself. No allowances are made for overhaul costs, although this may also be approximated by adjustment of the unit cost of fill.

Topsoil and seeding costs are based only on the sloping surface between the shoulder break and the toe of the fill. Stripping of the original ground surface is assumed to be necessary only for the width of the roadbed associated with the guardrail design treatment and is omitted from the analyses because it represents an equal-cost item for all roadside treatments and therefore cancels out when studying differences in costs between the alternative treatments.

The initial cost of guardrail should include the cost of end anchorages as well. Inclusion of anchorage cost is especially important for correct economy studies when guardrail installation lengths are short. For example, Figure 4 shows that if both ends of a 200-ft long

Case B, which is based on a different set of unit costs, shows a special case where equal-cost and equal-safety heights are identical, so that a clear-cut decision exists over the entire range of embankment heights.

Case C, based on still another set of unit costs, also yields the two clear-cut outcomes and also another trade-off zone that results from the equal-cost height exceeding the equal-safety height, thus producing a range of fill heights where flat slope is cheaper but guardrail is safer. Where the flat slope is 4:1 or flatter, this outcome will seldom occur unless the cost conditions are very unusual.

Construction Costs

The primary costs considered in this paper include the cost of fill, topsoil, seeding, and guardrail. The cost of fill is based on the volume

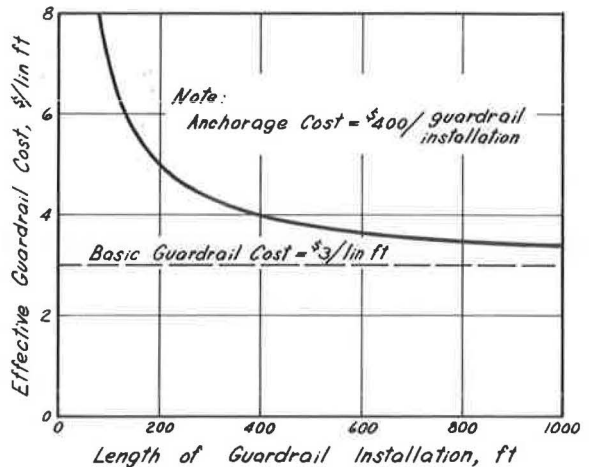


Figure 4. Effective guardrail cost.

section of \$3.00 per lineal foot guardrail are secured with anchorages costing \$200.00 each, the "effective" cost of the guardrail is \$5.00 per lineal foot when anchorage cost is prorated over the entire length of guardrail installation.

Additional right-of-way and culvert costs entailed by flat slope designs have been omitted from the general analyses that follow, but a few specific examples showing the effect of these costs on economic break-even heights are presented.

Maintenance Costs

The omission of maintenance costs results in underestimation of break-even heights for rail versus flattened slope. If maintenance cost data are unavailable or sketchy, NCHRP Report 42, "Interstate Highway Maintenance Requirements and Unit Maintenance Expenditure Index" (6), provides a convenient means for estimating maintenance costs associated with alternate roadside treatments. Maintenance practices vary somewhat among the states, resulting in different maintenance expenditures. However, it is safe to say that minimal maintenance standards for any maintenance item associated with the roadside probably result in some "compensating" cost to the highway agency sooner or later. Thus, failure to correct slope erosion may necessitate repairs to shoulders or excessive cleaning of roadside drainage ditches; failure to repaint guardrails as needed may result in earlier guardrail replacement because of corrosion.

Guardrail maintenance cost will vary with maintenance practices, type of guardrail (beam, cable), and guardrail surface or material (painted, galvanized, weathering steel). Painting is a major component of guardrail maintenance in colder regions, where corrosion from de-icing materials may necessitate repainting on a 2-year schedule. Repainting, including wire brush and hand scraping, costs about 40 cents per lineal foot per application (5). Expenditures are also necessary for repairs to guardrails damaged by collisions and snow-removal operations. There is of course some substitutability between first cost and maintenance cost, as for example with the use of higher cost weathering steels that do not require painting. Guardrail maintenance expenditures appear to average about 10 cents per lineal foot per year (6).

Mowing practices also vary widely among the states. The number of cuts per year and the limiting slope steepness beyond which mowing is not done are among the factors which affect mowing costs. Some states do not mow 2:1 slopes but rather allow "volunteer" growth to overrun the slope face. Other states mow 2:1 slopes once a year to help extend the grass root system and to leave a mulch on the slope over winter. This measure helps to prevent slope erosion damage (7). Some agencies still hand-trim around guardrails, although the trend is to apply soil sterilant to a 2-ft-wide strip under the rail. Soil sterilants usually remain active for a minimum period of 2 years and the cost of \$45 per mile per application is less than one-tenth the cost of hand trimming for the same period (7). Economic break-even heights are least sensitive to differences in vegetation control costs.

Erosion damage is another maintenance cost item that should be considered in studies of alternate roadside treatments. Erosion costs include not only repair of the slope itself but also the removal of erosion products from ditches and culverts. In addition, deposition of eroded materials in ditches and streams may increase the extent of damage from heavy rains to other roadway components and abutting property and, although this latter cost is extremely difficult to quantify, it is nevertheless one assignable to the steep slope design common with guardrail installation. NCHRP Report 42 provides separate erosion cost estimating equations for slopes 2:1 and steeper and for slopes flatter than 2:1. Although annual precipitation is the only independent variable used in these equations, the total erosion cost for a given sideslope would also be a function of embankment height.

Drifting of snow and consequent snow-removal costs have been shown to be strongly influenced by highway cross section design. In open country where the highway lies perpendicular to the predominant winter winds, embankments tend to be swept clear of snow if sideslopes are 4:1 or flatter. Steep sideslopes, particularly when the shoulder break area is not well-rounded, contribute to drifting problems through the formation of eddies. The more "streamlined" the cross section the less problem with drifting

snow. Thus guardrails also worsen drifting, especially when previous plowing has packed snow against the guardrail, transforming it into a 2-ft-high solid barrier. The turbulence in the wake of this obstruction may cause rapid snow deposition across the full roadway width because of the decreased carrying capacity of the turbulent eddies (8). NCHRP Report 42 provides a comprehensive analysis of snow-removal costs. The elimination of guardrail through slope flattening can probably reduce snow-removal costs on embankments by 15 to 20 percent.

In cases where cut slopes are flattened in nearby cut sections to provide the additional fill material needed to flatten a fill slope so that guardrail can be omitted, there may be an indirect maintenance benefit in the form of reduced erosion and drifting of snow on these cut slopes. The flattened cut slopes also increase roadside safety and in general are more natural in appearance and aesthetically pleasing in the same way that flat fill slopes are more attractive.

Annual Cost

Consideration of both construction and annual maintenance costs requires that costs be put on a common time basis. Embankment, topsoil, and seeding can be assumed to last for the economic life of the highway. Sections of guardrail, however, may require earlier replacement owing to damage from severe collisions. Replacement may also occur as a result of implementation of a new guardrail standard. A 20-year economic life is used for all construction cost elements in the following presentations unless otherwise noted, and a 6 percent interest rate was used to convert initial cost to annual cost.

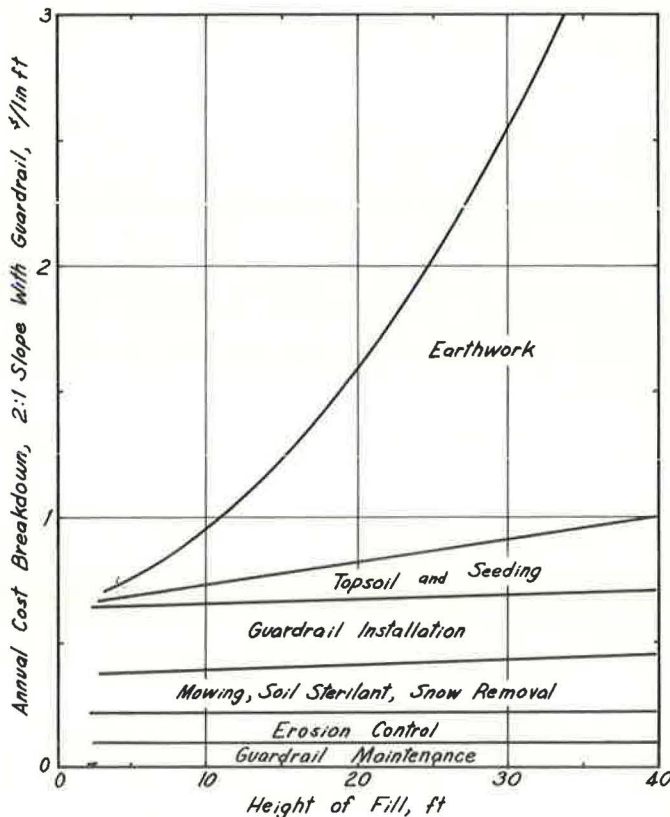


Figure 5. Annual cost breakdown for 2:1 slope with guardrail.

Figure 5 shows a total annual cost buildup for constant-height embankments for guardrail treatment with 2:1 slope. The maintenance costs could be considered "typical" for northern, humid areas. Fill cost is \$0.50 per cubic yard and guardrail is \$3.00 per lineal foot. The costs in this figure and elsewhere in this paper are for one roadside only. It can be seen that maintenance costs make up a considerable portion of the total annual cost for low to medium fill heights. For a 20-ft fill height, the cost of earthwork and guardrail combined accounts for only 65 percent of the total annual cost, while the combined maintenance cost is 26 percent, and topsoil and seeding 9 percent.

BREAK-EVEN ANALYSIS

Annual Cost Curves

Figures 6, 7, and 8 provide an insight into the relative economy of guardrail roadside design versus flattened slope design for three basic cases of embankment profile geometry. In each case the cross slope of the original ground is assumed to be zero.

Because of the complexities associated with estimation of total maintenance cost for both guardrail and flattened slope designs, the annual cost in these figures was based on differential maintenance cost—guardrail design less flattened slope maintenance cost. Since total maintenance cost for design with guardrail always exceeds that for flattened slope design, this difference has been added to the guardrail design. Therefore the annual cost curves for the flattened slope designs (3:1, 4:1, etc.) consist solely of fill,

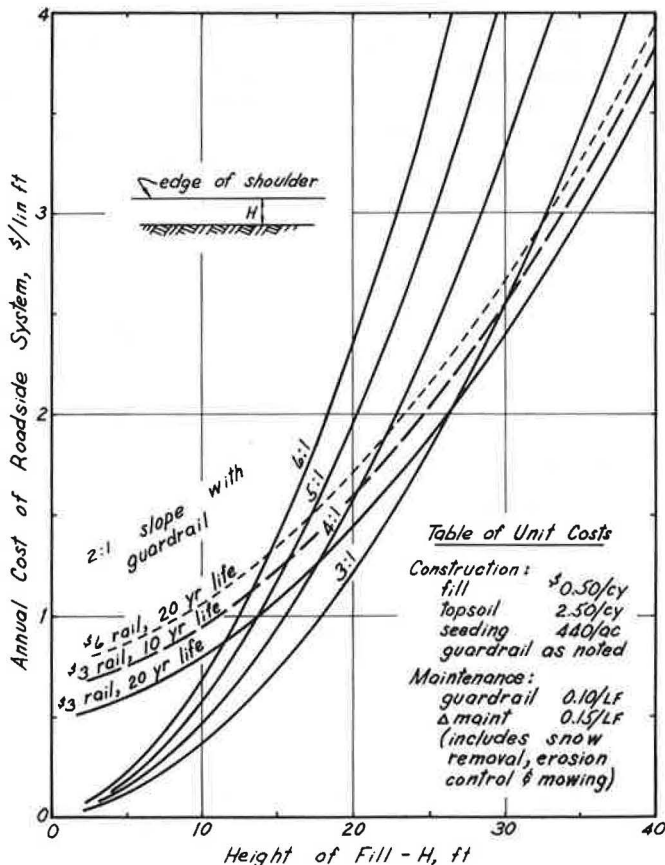


Figure 6. Annual cost per lineal foot for constant-height embankments.

topsoil, and seeding, while the guardrail design cost curves are the sum of fill, topsoil, seeding, and guardrail installation cost plus the amount by which the maintenance cost for guardrail design exceeds flattened slope maintenance cost. While this procedure underestimates total annual costs, it nevertheless permits investigation of the relative economy of the two basic roadside design treatments and determination of equal-cost embankment heights for the assumed unit costs.

Figure 6 shows annual costs for constant-height embankments. Note that for the particular unit costs used here, which are in no way extreme, a 6:1 design is cheaper than the alternative guardrail design up to a height of 12 ft, given a guardrail cost of \$3.00 per foot and guardrail life of 20 years. The 4:1 design is cheaper than guardrail up to a fill height of 18 ft. Many designers consider the 4:1 slope as the steepest acceptable slope from a safety standpoint if guardrail is not used, and yet most designers choose to install guardrail in preference to a 4:1 slope long before the economic break-even height is reached. A 3:1 design is cheaper than guardrail up to a fill height of 27 ft.

The effect of guardrail life assumptions is also shown in Figure 6. If guardrail is assumed to be replaced at the same initial cost after only 10 years, the break-even height for the 4:1 design increases by 2 ft (18 to 20 ft). Doubling the initial cost of guardrail with a 20-year life raises the break-even height from 18 to 22 ft for the 4:1 design.

The effect of maintenance cost assumptions can be readily explored in Figure 6. If the difference in annual maintenance costs between the 4:1 design and guardrail design is increased by \$0.20 per foot, making the total difference in maintenance costs \$0.45 per foot, the break-even height is raised from 18 ft to 21 ft for the \$3.00 guardrail with 20-year life.

Figure 7 shows annual costs per foot of embankment for embankments on a constant grade crossing a V-shaped valley or depression. The unit costs are the same here as in Figure 6, and again the cost is for one roadside only. Of course, a perfectly planar valley shape as assumed here is not likely to be found in nature, but it is felt that moderate departures in the original ground line from the plane surface assumption will not change break-even heights substantially from what they are here, and the relative costs of the alternate designs would probably be similar.

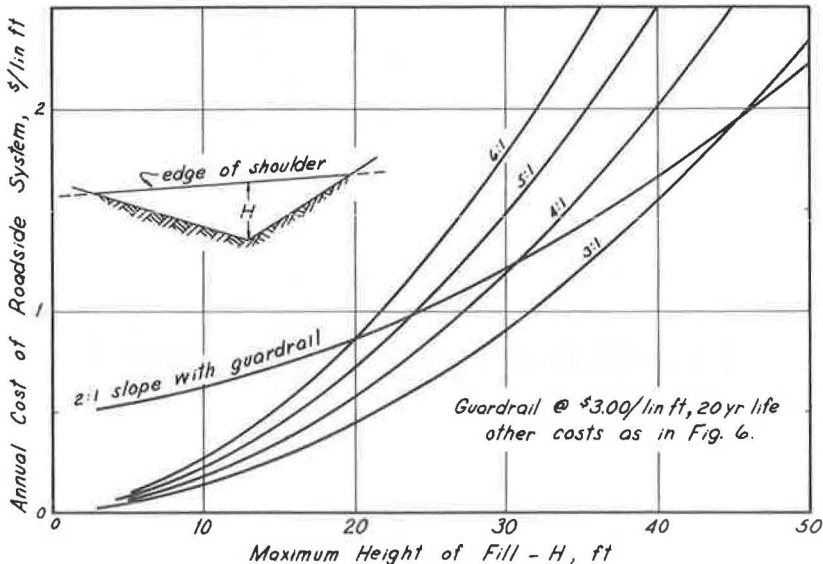


Figure 7. Annual cost per lineal foot for constant-grade embankments over V-shaped valley.

For any value of H (the maximum fill height at the vertex of the valley) one can determine the difference in total annual cost for the full embankment section for the guardrail design versus one of the flat slope designs by multiplying the annual cost difference found from Figure 7 by the length of the fill. It was assumed in this case and the following case in Figure 8 that guardrail is installed for the entire length of the fill. Although this is not always the case in practice, it is nevertheless a recommended treatment in steeper terrain (4). However, the break-even heights in Figure 7 also tell the designer at what fill height, as one proceeds toward the vertex, it becomes cheaper to steepen the slope and install guardrail.

It is quite apparent that break-even heights are much higher for the valley crossing than for the case of constant-height embankment examined in Figure 6. For example, for the constant grade over a V-shaped valley, 4:1 design is cheaper than guardrail treatment up to a maximum fill height of about 31 ft, whereas the corresponding break-even height for the constant-height embankment is only 18 feet (\$3.00 guardrail, 20-year life).

The width of the embankment is of importance in regard to right-of-way needs. At the 4:1 break-even height of 31 ft, the toe of the fill would lie 124 ft from the edge of the shoulder. However, this is the maximum distance to the toe of slope along the entire embankment, and for half of the embankment length the toe would be less than one-half this distance, or 62 ft away from the edge of the shoulder.

Figure 8 shows another idealization of a common case of embankment profile geometry: a sag vertical curve crossing a V-shaped valley with approach tangents coincident with the valley slopes. As would be expected, this case produces break-even heights that exceed those of the constant-grade embankment over the same terrain. For the 4:1 design, the break-even height is 38 ft whereas that for the constant-grade case was only 31 ft. The toe of the fill at the vertex lies 152 ft from the edge of the shoulder, but for half the length of the embankment the toe of the fill would be less than one-fourth of this distance from the shoulder, or 38 ft, owing to the geometry of the vertical curve.

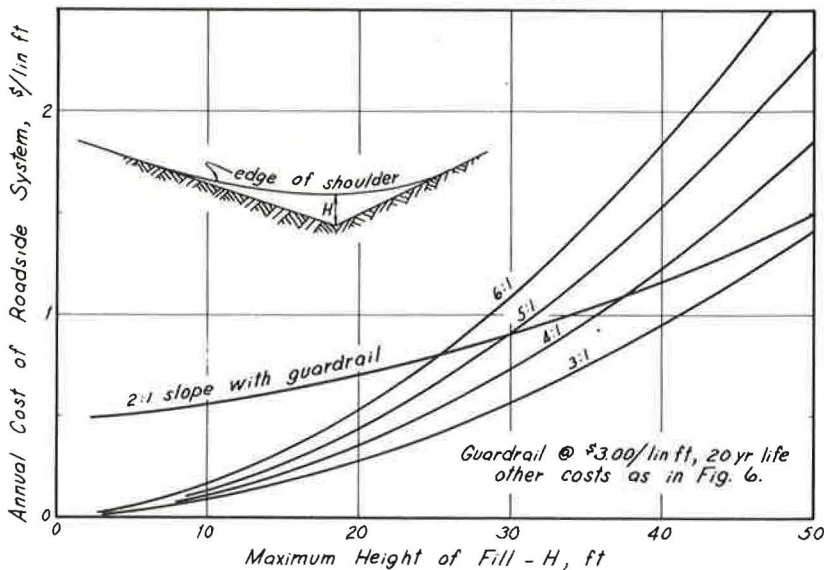


Figure 8. Annual cost per lineal foot for vertical curve embankments over V-shaped valley.

TABLE 1

RANGE OF ECONOMIC BREAK-EVEN HEIGHT, H, FOR THREE CASES OF EMBANKMENT PROFILE GEOMETRY^a

Embankment Profile Geometry	Sideslope			
	6:1	5:1	4:1	3:1
	6-14 ft	7-18 ft	9-23 ft	14-33 ft
	10-26 ft	12-31 ft	16-39 ft	24-57 ft
	13-34 ft	16-40 ft	21-51 ft	31-74 ft

^aBased on unit cost sets A and E, Figure 9.

Break-Even Charts

Figures 9, 10, and 11 show plots of economic break-even heights for five different sets of unit costs for the three cases of embankment profile geometry considered in Figures 6, 7, and 8 respectively. Each of the lettered curves gives the slope-height combinations for which the flattened slope design is equal in annual cost to design with guardrail with 2:1 slopes, for a particular set of unit construction and maintenance costs. Break-even heights can also be read off for nonintegral slope values, such as 3.5:1.

Curve A tends to favor guardrail installation because fill and topsoil unit costs are high, guardrail initial cost is low, and differential maintenance is assumed to be zero. Curve E is most favorable to flattening of sideslopes because fill and topsoil unit costs are low and guardrail initial cost and differential maintenance cost are both high.

Of interest is the considerable spread in break-even heights for any of the flat slopes corresponding to the different sets of unit costs, as given in Table 1. For the constant-height embankment the economic break-even height for the 4:1 design ranges from 9 to

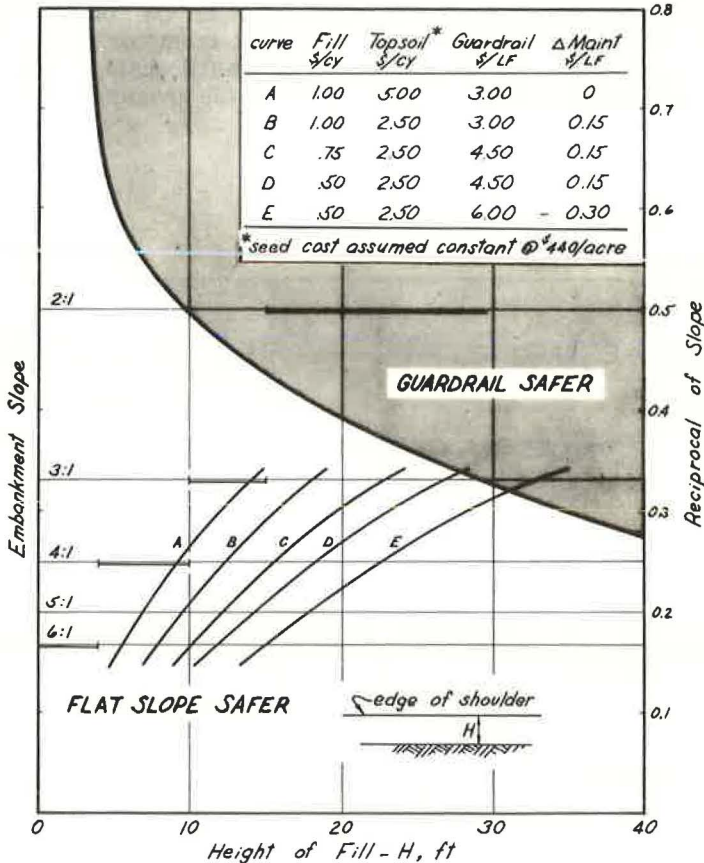


Figure 9. Break-even heights for constant-height embankments.

23 ft. The range is greatest for the 3:1 slope (14 to 33 ft) and smallest for the 6:1 slope (6 to 14 ft).

The economic break-even heights for the several sideslopes may be compared with AASHO's suggested sideslope-fill height values for flat or rolling terrain, which are shown as heavy lines in Figure 9. The AASHO maximum fill heights for each slope lie close to curve A, which represents costs most favorable to guardrail installation and might thus be considered somewhat conservative height limits (even with allowance for right-of-way costs at moderate land values, the effect of which is noted later in this paper).

The economic break-even curves for the constant grade over V-shaped valley (Fig. 10) are flatter and shifted further to the right than the corresponding curves for the constant-height embankment. This is even more pronounced for the case of the vertical curve over the V-shaped valley (Fig. 11). Table 1 summarizes the range in break-even heights for all three cases of embankment geometry. The ranges are based on the two extreme unit cost curves, A and E. Examination of Table 1 reveals that break-even heights for the constant grade, and vertical curve embankments over a V-shaped valley are about 75 percent and 125 percent greater respectively than those for the constant-height embankment. Therefore, application of guide values for economic break-even heights based on constant-height embankments to design situations involving profiles similar to the V-shaped valley could often result in selection of guardrail treatment for the roadside, when in fact the flattening of sideslopes would be a much cheaper alternative.

In order to compare economic break-even height with "equal-safety" height, the California equal severity index curve has been plotted in Figure 9. The shaded area above the curve represents those sideslope-embankment height combinations for which guardrail should be used from the safety standpoint, while the area below the curve favors flattened slope treatment for greater safety. Over the broad range of cost assumptions in Figure 9 the economic break-even height is less than the equal-safety, or safety break-even height except for 3:1 slopes at very large heights and at unit costs

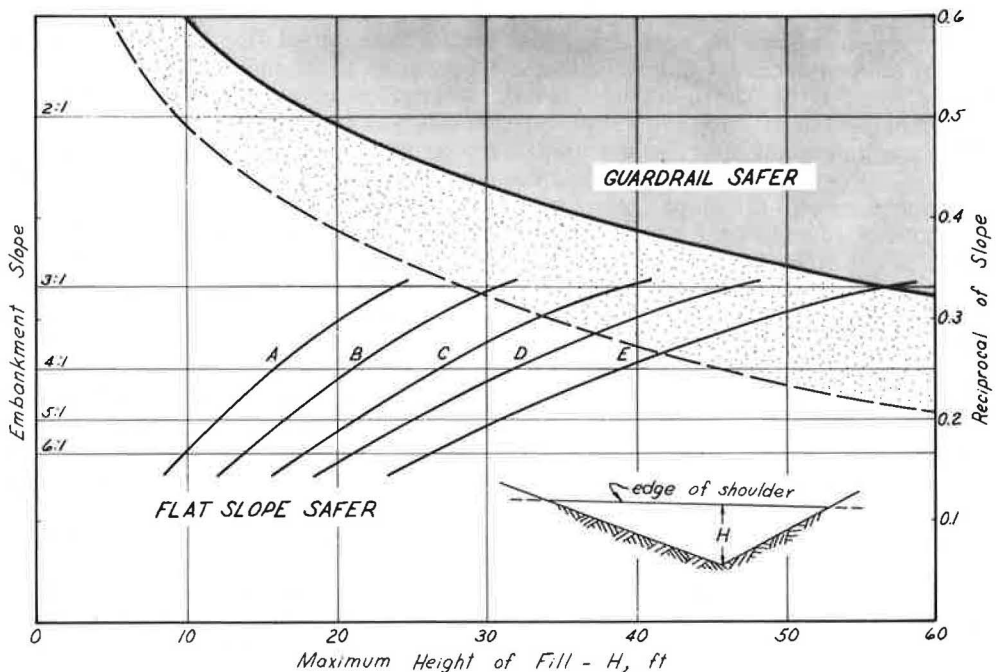


Figure 10. Break-even heights for constant-grade embankments over V-shaped valleys.

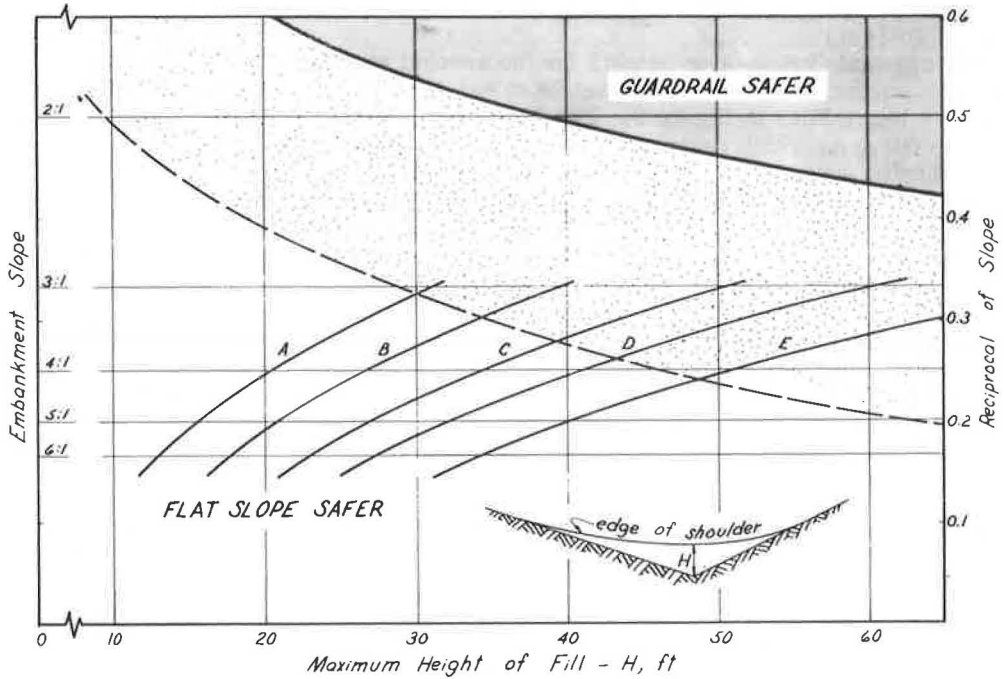


Figure 11. Break-even heights for vertical curve embankments over V-shaped valleys.

highly unfavorable to guardrail roadside treatment. Curve C, which is based on "intermediate" costs, shows the economic break-even height for 4:1 slope to be 16 ft, although the equal severity concept indicates that a 4:1 slope is safer than guardrail up to a fill height of about 47 ft. There is thus a sizable interval of embankment height where guardrail is cheaper but 4:1 slope is safer. Within this height range the designer must judge whether the safety advantage of 4:1 slope over guardrail merits the additional cost. In such cases, the more highly trafficked the road, the more one could justify the extra cost associated with 4:1 slope treatment.

In Figures 10 and 11 the equal severity index curve is plotted as a dashed line because it is not directly applicable to these two embankment profiles, since fill height changes continuously over these embankments. Thus an embankment of given sideslope having a maximum height (at the vertex) that lies on the curve is equal in hazard to a guardrail treatment only at that point; at all other points along the embankment it is safer to omit guardrail, and so the overall hazard of such an embankment is less than if guardrail were installed over its entire length. To account for this factor the equal severity index curve has been shifted upward on the assumption that the median height of the embankment better approximates the height-sideslope severity index when fill height varies uniformly over the embankment's length. The median height corresponds to the height that is exceeded over half the length of the embankment. In the case of the constant grade over the V-shaped valley the median height is equal to one-half the maximum height, while for the vertical curve alignment it is one-fourth the maximum embankment height. This results in a greater translation of the original equal severity index curve in the case of the vertical curve alignment than in the constant-grade case. Although these adjustments are somewhat arbitrary, they are in the "right direction", and it is believed that the darker area above the adjusted curves better reflects those slope-height combinations for which guardrail is safer. The adjusted curves result in a greater disparity between the economic break-even heights and the safety break-even

heights for varying fill-height embankments than in the case of the constant-height embankment, and the "trade-off" height intervals (guardrail cheaper but flattened slope safer) are increased.

Effect of Other Cost Factors


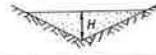
It can be shown that the inclusion of right-of-way cost has little effect on economic break-even heights for the lower land values typical of most rural areas. Table 2 shows the break-even heights for right-of-way values of \$1,000 and \$2,000 per acre, along with the break-even height that obtains when right-of-way cost is omitted. The analysis is for the 4:1 slope versus guardrail design, and the unit costs are those of Figure 7. Additional right-of-way width is here defined as the difference in the distances from the edge of shoulder to toe of slope for the two alternative designs. The effect of right-of-way cost is to reduce the break-even heights by only about 1 to 2 ft per \$1,000 per acre of land value for both of the cases of embankment profile geometry. Of course, with a slope of 4:1 or flatter it may be possible to obtain easements whereby agricultural uses are permitted on the outer portion of the long slopes generated by the flat embankments, thereby reducing right-of-way cost.

The effect of slope flattening on culvert costs and resulting economic break-even height is probably the most significant factor that has thus far been omitted from the analysis. The annual cost curves can still be used to determine break-even heights if the additional culvert cost is divided by the length of the embankment, then converted to an annual cost, and then graphically added to the appropriate flat-slope cost curve. Table 3 shows the effect of two assumed culvert unit costs for a 400-ft long constant-grade embankment over a V-shaped valley. The culvert is assumed to be located at the point of maximum fill height (vertex of the valley). Culvert costs of \$20 and \$40 per lineal foot (which might be typical for 48-in. and 60-in. diameter corrugated metal pipe culvert) significantly reduce the break-even height when compared to no allowance for culvert cost. Nevertheless, the break-even heights are still greater than what many highway designers apparently estimate them to be. Of course, the effect of culvert cost is reduced as the length of the embankment section increases.

Where the highway crosses a steep-bottomed draw, it may be quite economical to completely fill in the pocket between the embankment and the uphill portion of the ravine, since this treatment can often reduce the length of the culvert by permitting it to be located near the end of the fill where the width is narrow (if not obviating the need for a culvert entirely), and guardrail can be omitted (9). Safety is increased as well.

Guardrail anchorage cost also affects economic break-even height. The annual cost and break-even height curves in Figures 6 through 11 can be used with allowance for

TABLE 2
EFFECT OF RIGHT-OF-WAY COST ON
ECONOMIC BREAK-EVEN HEIGHT, H^a

Right-of-Way Cost per Acre, \$	Embankment Profile Geometry	
		
0	17.7 ft	30.7 ft
1,000	16.7 ft	29.1 ft
2,000	15.7 ft	27.5 ft

^a4:1 slope vs. 2:1 slope with guardrail; unit costs as given in Figure 7.

TABLE 3
EFFECT OF CULVERT COST AND GUARDRAIL ANCHORAGE
COST ON ECONOMIC BREAK-EVEN HEIGHT^a

Culvert Cost per Lineal Foot, \$	Guardrail Anchorage Cost Omitted	Guardrail Anchorage Cost Included ^b
0	30.5 ft	33.5 ft
20	24.2 ft	26.6 ft
40	19.5 ft	21.7 ft

^aConstant grade embankment over V-shaped valley, 400 ft long, 4:1 slope vs. 2:1 slope with guardrail; unit costs as given in Figure 7.

^bTwo anchorages at \$200 each.

anchorage cost if the effective guardrail cost (anchorage cost converted to a per-foot-of-installation basis and added to the basic cost of guardrail) corresponds in value to the guardrail costs used in these charts. The effect of including anchorage cost in the preceding example is shown in the last column of Table 3. The effect of anchorage costs increases as the length of fill decreases, and for short embankments of the order of 200 or 300 ft in length the economic break-even height for flat slope treatment may increase by 3 or 4 ft, depending on anchorage design practice and cost.

SUMMARY AND CONCLUSION

The economic break-even heights for flattened fill slopes versus installation of roadside guardrail vary considerably with unit costs of construction and maintenance and type of embankment profile. Economic break-even height is generally well below the safety break-even height, which results in a fairly wide span of fill heights over which guardrail installation is cheaper than slope flattening, but design with flattened slope is safer. Economic break-even height for embankments of smoothly varying height are significantly greater than those for constant-height embankments. Right-of-way cost in rural areas is likely to have little effect on break-even height, while culvert cost can significantly lower it.

Considering what the authors believe to be an excessive use of roadside design with guardrail over embankments on rural highways and at interchanges, it appears that many designers tend to underestimate the economic break-even height for flattened sideslopes. Preparation of a series of break-even curves such as those presented here would be helpful in permitting quick approximate study of embankment sections for proper selection of roadside design treatment. The analysis method can also easily be programmed for computer use along with routine earthwork calculations. More careful evaluation of alternative roadside treatments can produce substantial reductions in total annual highway cost as well as improve highway safety and aesthetic appearance.

REFERENCES

1. Glennon, John C., and Tamburri, Thomas N. Objective Criteria for Guardrail Installation. Traffic Department, California Division of Highways, Sacramento, July 1966.
2. Guardrails, Barriers and Sign Supports. Highway Research Record 174, 1966.
3. A Policy on Geometric Design of Rural Highways. American Association of State Highway Officials, Washington, D. C., 1965.
4. Highway Guardrail: Determination of Need and Geometric Requirements, With Particular Reference to Beam-Type Guardrail. HRB Special Report 81, 1964.
5. Cardone, S. M. Galvanizing Reduces Bridge Rail and Guardrail Maintenance in Michigan. Highway Research Record 11, 1963, pp. 62-65.
6. Bertam D. Tallamy Associates. Interstate Highway Maintenance Requirements and Unit Maintenance Expenditure Index. NCHRP Report 42, 1967.
7. O'Brien, Robert W. Effect of Contract Mowing on Massachusetts Maintenance Costs. Highway Research Record 11, 1963, pp. 23-49.
8. Cron, F. W. Snowdrift Control Thru Highway Design. Public Roads, Dec. 1967, pp. 227-234.
9. Cron, F. W. Slope Design Practice in the Great Smokey Mountain National Park. HRB Report of the Committee on Roadside Design, 1948, pp. 32-43.

Space Technology for Auto-Highway Safety

M. A. KAPLAN, R. J. HENSEN, and R. J. FAY,
Department of Mechanical Sciences and Environmental Engineering,
University of Denver

A research team is engaged in the development of attenuation systems for highway gores. The achievements to date and future aims are reported. A method for initially screening available energy-absorbing devices is presented. The evaluation of the remaining devices by testing and analysis is discussed. The procedures for inexpensive and flexible testing of attenuation systems using scale-modeling techniques are developed.

•THE University of Denver is engaged in a multidisciplinary research effort to establish the technical, economic, and marketing feasibility of selected unused patents held by the National Aeronautics and Space Administration (NASA). This program, which is sponsored by NASA, is a three-year pilot demonstration of the potential value of using faculty-student design teams to effect the transfer of NASA-developed technology to the public sector. It involves students, faculty, and research personnel from each of the colleges within the university.

The fact that NASA holds a number of patents on energy-absorbing devices made it seem that this area would contain a sufficiently broad spectrum of patented concepts for the program. A current awareness of highway safety needs makes energy-absorbing devices very timely (1). This awareness was pointed out in a paper given at a recent highway engineering conference (2). The paper states in part:

... the single vehicle "ran off the road" accident is a leading source of fatalities on our Interstate system. . . . Elevated gore structures such as exit ramps on bridges are a prime example. The rather hostile nature of the nose of the bridge parapet and railing in such an area involving driver decisions at freeway speeds, and the large number of such structures in urban areas with high average daily traffic figures have combined to make real problem areas of such structures. . . . Impact energy absorption barriers can be used to reduce the severity of these hazards. Conventional guardrail installations are not well suited for such areas, inasmuch as they are best suited for glancing impacts and are not satisfactory for the kind of high speed, near head-on collision which may occur at these sites.

Significant efforts to protect vehicle occupants from the lethal effects of impacting a fixed roadside obstacle were initiated by the Bureau of Public Roads in December 1966. Under a program entitled "Structural Systems in Support of Highway Safety", a short-range study was initiated to develop a first generation of attenuators based largely on full-scale impact tests of systems developed from existing technology (3). The criteria established for evaluating the tests were limited to preliminary estimates of vehicle weight ranges, maximum impact speeds, maximum angle of impact, and maximum average passenger deceleration rates. This program has resulted in the evolution of a number of devices that provide varying degrees of impact attenuation (4). However, these devices are still in the experimental stage and are subject to continual change. Also, a lack of information on adequate performance and cost criteria has

Paper sponsored by Committee on Guardrail, Median Barriers and Sign, Signal and Lighting Supports and presented at the 49th Annual Meeting.

made it almost impossible to establish design standards. Thus existing devices are each designed according to different criteria, making it very difficult to compare their performance characteristics and overall cost factors. Based on this appraisal of the state of the art, it was decided that the NASA study would concentrate on patents in the area of energy-absorbing devices, directing a portion of our efforts toward two aspects of auto-highway safety: applications to the automobile structure, and applications to the fixed highway system. This paper concentrates on the latter area.

THE BASIC PROBLEM

The division of the roadways on an elevated bridge structure necessarily creates an intersection of parapets and railings of the respective roadways. The critical problem in terms of impact attenuation is at this intersection or gore area as shown in Figure 1. The shaded area can be designed either as a recovery zone or as an attenuation and/or redirection zone. Under normal conditions, vehicles pass to one side or the other of this zone; but in the event of an erratic maneuver caused by driver indecision or confusion, the vehicle may well enter the zone. If the vertical and horizontal alignment of the roadways permit the zone to be large enough, the driver may be able to bring his vehicle under control without striking the parapet along the edge of the structure. However, in most situations the available area is too restricted, thus making it necessary to redirect or stop the vehicle with tolerable decelerations to the occupants and minimum conflict with other vehicles traveling in the lanes adjacent to the gore area.

THE ATTENUATION SYSTEM

Protection from gore impacts can be provided by a buffering system. Such a system is composed of individual energy-absorbing devices, tie-down and connecting elements, and load-distributing elements.

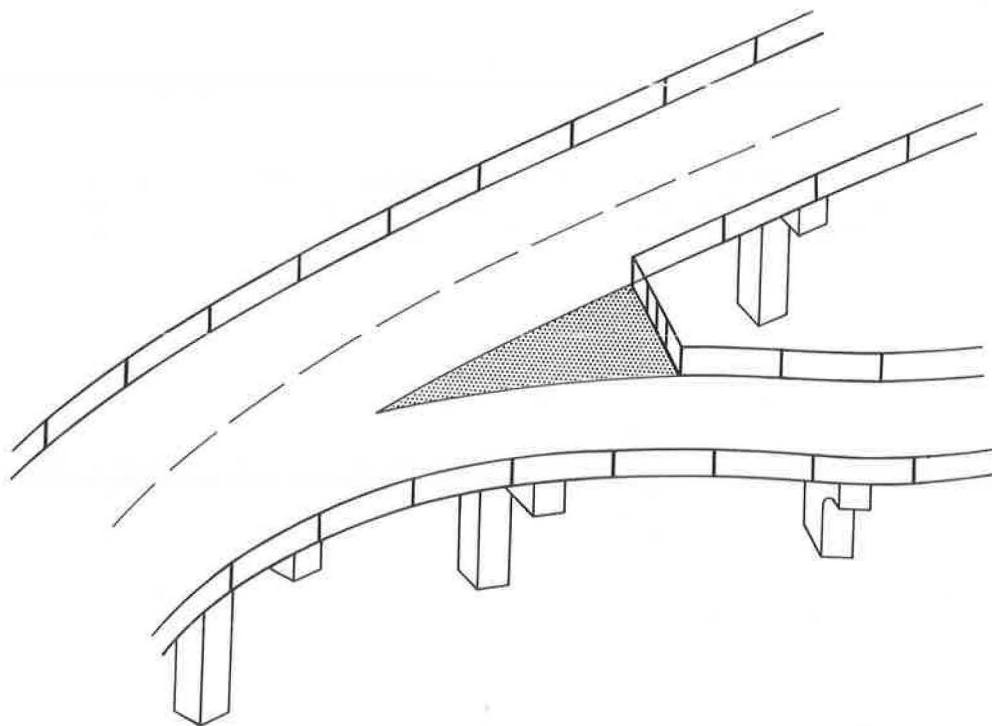


Figure 1.

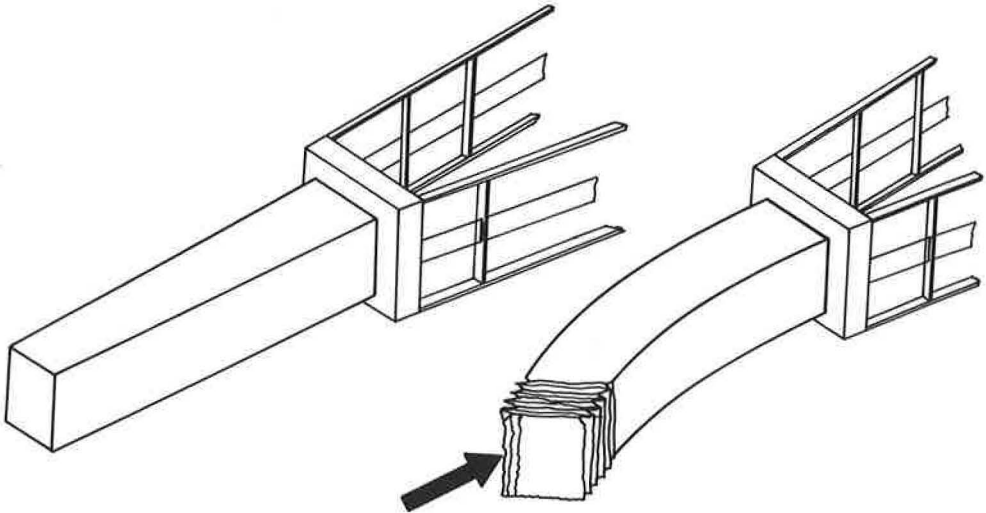


Figure 2.

A generalized attenuation system is shown in Figure 2. The system is somewhat like a structural column that must absorb axial loads in stopping the vehicle, and bending and shear forces in redirecting the vehicle. It must also absorb shear and bending on the vertical plane to compensate for eccentric loading due to differences in the relative heights of the mass centers of the vehicle and the attenuation system.

The magnitudes of the axial and shear forces imparted to the attenuation system by the vehicle are a function of the weight and speed of the vehicle, the angle of impact, and the point of impact. The actions of the vehicle during an impact are largely a function of the reacting forces generated by the attenuation system. Axial deceleration is governed by the collapse of the system, and redirection is controlled by the bending and shear resistance.

IDENTIFICATION OF PERFORMANCE CRITERIA

Operational buffering systems cannot be properly designed nor adequately tested until performance-design criteria have been established. To date, there are insufficient data on vehicle dynamics and driver responses during an actual impact to fully define such criteria. Full-scale simulated crash tests have been used to evaluate a number of the vehicle dynamic characteristics and passenger deceleration forces (5, 6). However, the prohibitive costs and physical danger involved in such tests have not allowed testing over a wide range of conditions. In addition, the majority of such tests have presumed no driver response and a linear path of the vehicle prior to impact.

The "4-S" program of the Bureau of Public Roads referred to earlier has defined a partial set of criteria for purposes of evaluating the results of full-scale crash tests (3). However, these criteria are not inclusive in terms of performance standards. Three major criteria have yet to be defined in terms of attenuator design. The first is the range and probability of vehicle dynamic conditions prior to impact. Cost-effective design must necessarily be based on the majority of actual conditions rather than all possibilities or only those that are easily tested in a simulated crash. It is suggested that the evasive actions of a driver prior to impact will significantly modify the dynamic response observed in driverless test vehicles.

A second set of criteria to be evolved should consider the relationship between the time-deceleration history of the vehicle as shown in Figure 3 and resulting injury potential to the occupants. Only through effective measures (indexes) of injury exposure based on probable human tolerances will there be an adequate definition of deceleration

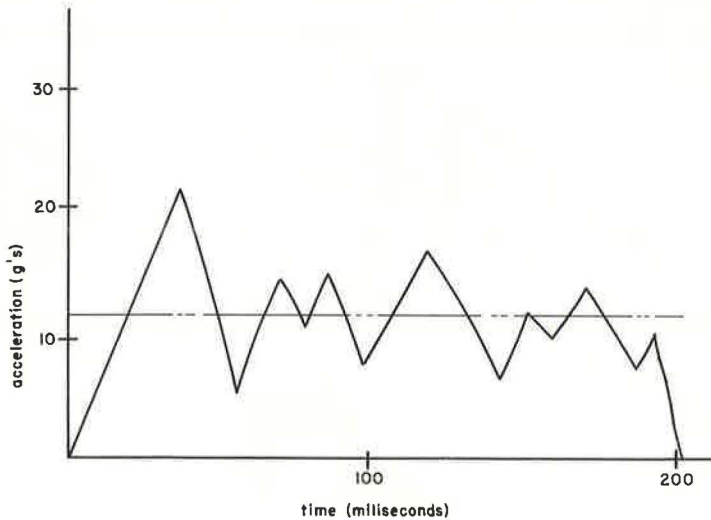


Figure 3.

constraints for attenuation systems. Without such defined constraints, valid comparisons of cost-effective designs are not possible.

The third set of criteria relate to the action of the vehicle during and after impact. No limitations on redirection angles or angular momentum imparted to the vehicle by the attenuation system have been established. Since the majority of bridge gore situations occur on heavily traveled freeways, the action of the vehicle after impact may, in fact, be of greatest concern in terms of overall safety of the freeway system.

With the availability of performance criteria, it will no longer be necessary to evaluate subjectively the "effectiveness" of particular buffering systems. Systems shall be termed either effective or not effective depending on whether or not they satisfy the existing performance criteria. System selection among the effective systems may then be made on the basis of size and total cost, i. e., some combination of initial and maintenance costs.

THE BUFFERING SYSTEM

In practice, a complete buffering system (one gore buffer) is a fairly complex arrangement of energy-absorbing units and tie-down, interconnecting, and load-distributing elements. Attempts to design a buffering system to meet accepted performance criteria will, therefore, be difficult and will probably involve some degree of trial and error. Recognizing this, we have attempted to simplify the design problem by formulating some rough guidelines. We feel that buffers meeting these requirements will be more likely to satisfy a reasonable set of performance criteria:

1. The buffer mass activated at impact should be small compared to the weight of the impacting vehicle.
2. The impacting vehicle should be assumed to be rigid.
3. The force-displacement curve of the barrier should be optimal or near optimal.
4. Buffer deformation and motion should be localized to the immediate area containing the impacting vehicle.
5. The buffer should not eject material onto the traveled roadway.
6. The buffer should not store mechanical energy.
7. The center of gravity of each portion of the attenuator should be above the center of vehicle load application.

8. The buffer should not produce significant angular accelerations until the vehicle has been entrapped.

9. The lateral stiffness of the barrier should be greatly increased near its base.

At the moment of impact, the portion of the buffer in direct contact with the vehicle and the vehicle itself are rapidly brought to a common velocity. When the ratio of barrier mass activated at impact to vehicle mass is not small compared to unity, then this common velocity is significantly different from the vehicle's initial velocity, and large deceleration forces occur. It follows, for example, that buffers should not be designed with massive rigid bumpers (guideline 1).

The deceleration forces imposed on the passenger compartment after impact depend on the stopping force provided by the buffer as well as the crushing characteristics of the front end of the vehicle. Front-end crushing is not easily incorporated into buffer design because of the variation in crushing with vehicle make and model. Thus it is believed that vehicle crushing should be ignored in buffer design, i. e., it should be assumed that the impacting vehicle is rigid (guideline 2). This assumption provides a margin of safety, since vehicle crushing attenuates the forces felt in the passenger compartment. Full-size or scale-model acceptance testing could then be conducted with specially constructed rigid vehicles. The test vehicles would be reusable and comparisons between different tests would become more meaningful.

Vehicle response after buffer impact must be such that acceptable levels of human tolerance are not exceeded. This condition places an upper bound on allowable force levels and therefore on the force-displacement response of the buffer. The force-displacement curve for which the acceptable limits of human tolerance are attained (but not exceeded) at all times during the deceleration process is called the optimum force-displacement curve.

To illustrate, consider the simple criterion that the g loads on the vehicle not exceed some constant value \bar{g} . The buffer must safely stop all vehicles traveling less than \bar{v} fps and weighing between W_0 and W_f lb. The initial force F_0 cannot exceed $W_0\bar{g}$ until the lightest vehicles have been stopped. Thus the optimum force-displacement curve is constant at F_0 until the kinetic energy of a vehicle of weight W_0 traveling at velocity \bar{v} has been dissipated. Equating the energy dissipated to the area under the force-displacement curve gives the penetration or stopping distance, $D_0 = \bar{v}^2/64.4\bar{g}$. Beyond D_0 the optimum curve rises continuously, since the force level may be raised without exceeding \bar{g} on the heavier vehicles that remain. The equation governing the shape of the optimum curve beyond D_0 is

$$F_0 D_0 + \int_{D_0}^X F(\bar{X}) d\bar{X} = \frac{W}{64.4} \bar{v}^2 \quad (1)$$

where X is the distance necessary to stop an impacting vehicle of weight W traveling at the maximum velocity \bar{v} . The left side of Eq. 1 is the work done on the buffer, while the right side is the maximum kinetic energy of a vehicle of weight W . At the point X where the vehicle has been stopped the force must produce the maximum allowable g load, i. e., $F(X) = W\bar{g}$. Substituting this into Eq. 1 and solving the resulting integral equation yields the optimum force-displacement relation for $X > D_0$:

$$F(X) = W_0\bar{g} \exp \left[64.4\bar{g}(X - D_0)/\bar{v}^2 \right] \quad (2)$$

The complete optimum force-displacement curve for this example is shown in Figure 4. The distance required to stop a vehicle of weight W impacting at \bar{v} fps is found by letting $F(X) = W\bar{g}$ in Eq. 2 and solving for X . The result is

$$X = \frac{\bar{v}^2}{64.4\bar{g}} \left(1 + \log \frac{W}{W_0} \right) \quad (3)$$

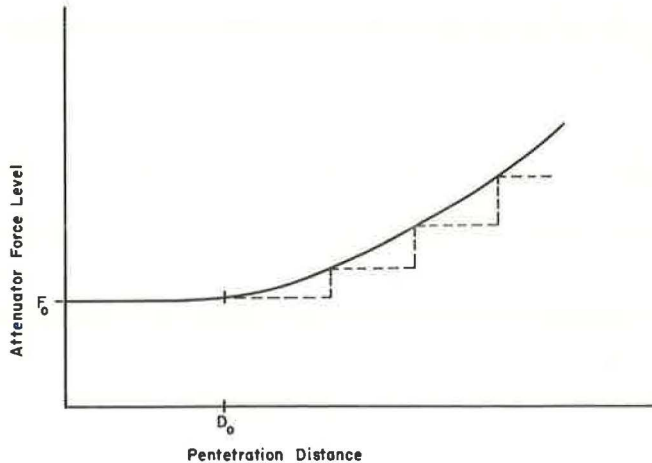


Figure 4.

The minimum stopping distance that the barrier must provide is found by putting $W = W_f$ into Eq. 3.

In practice, it will not often be feasible to design a barrier with an optimum force-displacement curve. However, the optimum curve may readily be approximated by designing the buffer as a series of energy-absorbing units whose components operate at different force levels, as shown by the dashed curve in Figure 4.

Consider two buffers designed with optimum (OP) and non-optimum (NOP) force-displacement curves respectively. The force-displacement curve of NOP must be below the optimum curve (or the design criteria will be violated), and therefore buffer NOP dissipates less energy in a given displacement than buffer OP. Since both buffers must be capable of dissipating equal amounts of energy, the minimum stopping distance provided by buffer NOP is greater than that provided by buffer OP. Other things being equal, buffer NOP will be larger than buffer OP, with the difference in size proportional to the variation of NOP's force-displacement curve from the optimum.

In order to maintain simplicity in the example, we ignored many effects—e.g., dynamic loads, multi-directional response, and dependence of injury on the time integral of a function of acceleration. The inclusion of these effects does not change the basic facts that the operating force levels of a buffer are constrained by the performance criteria and that the size of a buffer is minimized by optimizing its force characteristics within this constraint (guideline 3).

The importance of size in attenuator design follows from the consideration that smaller buffers will have a simpler support structure, a lower frequency of impact, and increased probability of acceptance for use in existing gore areas with limited placement area. A second parameter that is important in determining buffer size, namely, the length/stroke ratio, will be discussed in the next section.

The impact of a vehicle with a gore attenuator should not create a hazardous environment for those vehicles in the vicinity of the impact area. Therefore, the impact should not move the buffer so that it interferes with the flow of traffic (guideline 4). It should not eject material onto the roadway (guideline 5). Furthermore, the impacting vehicle should not, under most conditions, be allowed to reenter the roadway. In a direct or semi-direct hit on the buffer, the driver is not likely to be in full control of the vehicle and the vehicle itself will be at least partially disabled by the impact. The most likely means of a vehicle escaping from the buffer after impact are by elastic rebound, ramping, and spinout. Elastic rebound is easily controlled by selecting energy-absorbing units that dissipate rather than store energy (guideline 6). To prevent

ramping, the center of gravity of the individual units in the buffer must not be lower than the center of force application, so that the units have no tendency to rotate under the vehicle (guideline 7). Spinout is the most difficult of the three escape mechanisms to control. Spinout may occur when the vehicle, with no initial angular velocity, impacts the buffer off center. The resulting moment produces angular accelerations that can rotate the vehicle out of the barrier. Spinout may also occur with an initially spinning vehicle that is simply redirected by the buffer. We feel that the probability of spinout in both these cases will be greatly reduced if the outside of the buffer is readily deformable under relatively small forces (guideline 8). Under these circumstances, the buffer should tend to wrap around the vehicle without redirecting it. As the vehicle penetrates to the stiffer part of the buffer, the tendency toward spinout will be decreased by the lateral and friction forces provided by the material enclosing the front end of the vehicle.

In circumstances where the buffer cannot safely arrest the vehicle, it must be redirected. Large local deformations at redirection locations are undesirable. The buffer must therefore be designed with increased lateral stiffness in these areas (guideline 9).

SELECTION OF DEVICES FOR USE IN GORE BUFFERING SYSTEMS

Most of the available energy-absorbing devices can be engineered to operate over a wide range of force and energy levels. Devices with this type of flexibility will, in all probability, be incorporable into an effective attenuation system. Comparison between devices, therefore, will generally be made on the basis of their effect on total system cost.

The initial phase of our program was concerned with identification of those characteristics of an individual device that play an important role in the cost of the attenuation system. Our purpose was to provide a means of qualitatively comparing the 53 different devices with which the program was begun without the expense of system design, fabrication, and testing. The characteristics discussed in the following were concluded to be of major importance.

Reliability

Gore attenuators are required to operate over a wide range of environmental conditions during a time period measured in years. Some devices are virtually insensitive to weather and time effects and require no special care. Devices, however, that rely on friction and/or close tolerances for proper operation and devices that contain weather-sensitive materials will require special care to ensure reliability. This will be reflected in higher unit costs.

Cost of Manufacture and Assembly

The relationship of the cost of manufacture and assembly to initial cost is obvious. Devices that use standard materials and do not require close tolerances tend to have low manufacturing costs. Those devices that use off-the-shelf items are particularly attractive in this regard.

Reusability

Devices that are completely or partly reusable can be expected to exhibit lower maintenance costs.

Multi-Directional Load Capability

Buffer impacts occur over a range of positions and directions. Proper functioning of devices that only operate under a restricted range of loading directions requires the use of support and load-directing structures that add to system cost.

Material Efficiency

Material efficiency is defined as the energy absorbed per pound of device. The minimum weight of a buffer is the total energy to be dissipated divided by the material

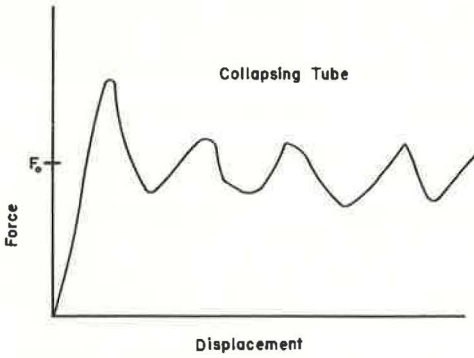
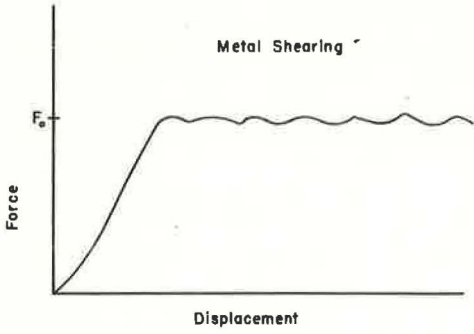


Figure 5.

efficiency of the basic device. Devices with low material efficiency tend to have high material costs.

There is a large variation in material efficiency with changes in materials and geometry. In general, however, when the weight of the deformed material is not a significant percentage of the total weight of the device, material efficiency is low.

Force-Displacement Curve and Length/Stroke Ratio

The force-displacement curve and length/stroke ratio have been grouped because together they determine approximately the minimum size of the attenuation system. System cost increases with size because of the increase in necessary supporting structure (including the foundation or pad for the attenuator) and the increase in maintenance costs due to a higher frequency of impact. We have already discussed the role of the system force-displacement curve in determining size. In order to design a buffer, the force-displacement relationship of the individual devices as a function of material properties, geometry, and direction of load ap-

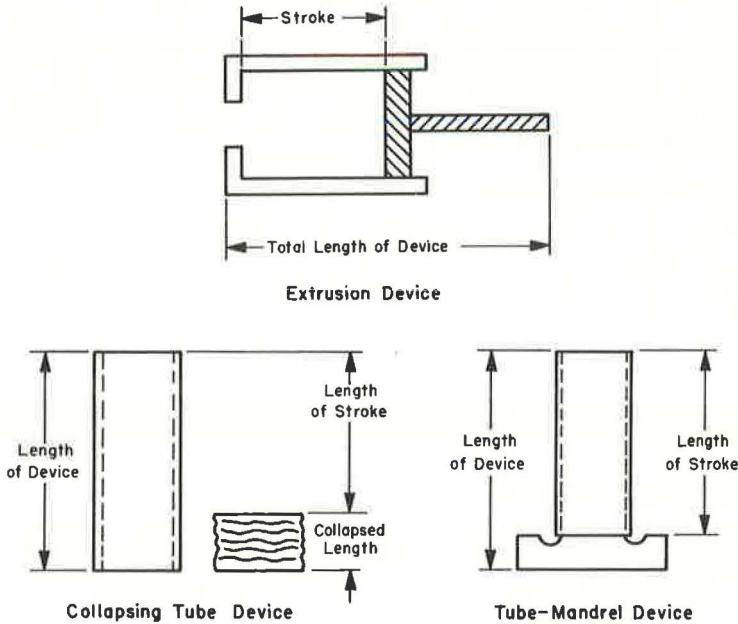


Figure 6.

plication must be known. These are determined by a combination of analysis and experimentation. Typical force-displacement curves (for a folding tube and metal shearing device) under axial loading are shown in Figure 5. The oscillatory nature of these force-displacement relationships is common to many energy-absorbing devices.

The maximum useful displacement provided by a device is called its stroke. The strokes of three energy-absorbing devices are shown in Figure 6. The minimum length of a device necessary to produce 1 foot of stroke is its length/stroke ratio. The minimum length of an attenuation system is the product of the minimum stopping distance that must be provided and the length/stroke ratio of the device being used in the system.

The use of these characteristics has enabled us to eliminate most of the original devices from consideration for use in attenuating systems for gores. The five patents that survived this critical review are the frangible tube, the collapsing tube, a metal strip bending device, a metal shearing device, and an extrusion device. We are also considering other energy-absorbing devices that have been invented during the course of the program.

Current Research Program

The properties of the selected energy-absorbing devices are being developed by analytical and experimental analysis. The knowledge generated by these studies will be used in the design of highway buffers. Scale models of these highway buffers will be built and tested.

Experimental Studies

Experimental evaluations of the energy-absorbing devices are being made using both quasi-static and dynamic tests. The quasi-static tests are performed with a hydraulically operated testing machine equipped with electronic instrumentation that records forces and deflections. This equipment, with the exception of the electronics, is standard equipment in most materials testing laboratories. Dynamic testing is also required to define the dynamic characteristics of absorbing devices. A unique dynamic testing machine was designed and constructed for this purpose. This testing machine, shown in Figure 7, is equipped with a 35-lb ram that is accelerated to speeds of up to 60 mph by a specially designed pneumatic cylinder. Directional control of the ram is provided by shock-mounted linear bearings that operate on hardened rods. The testing machine is equipped with a test specimen mounting table supported on shear pins that release the table in the event of an overload; the energy in the system is then absorbed by a hydraulic shock absorber positioned under the table. Electronic instrumentation provides

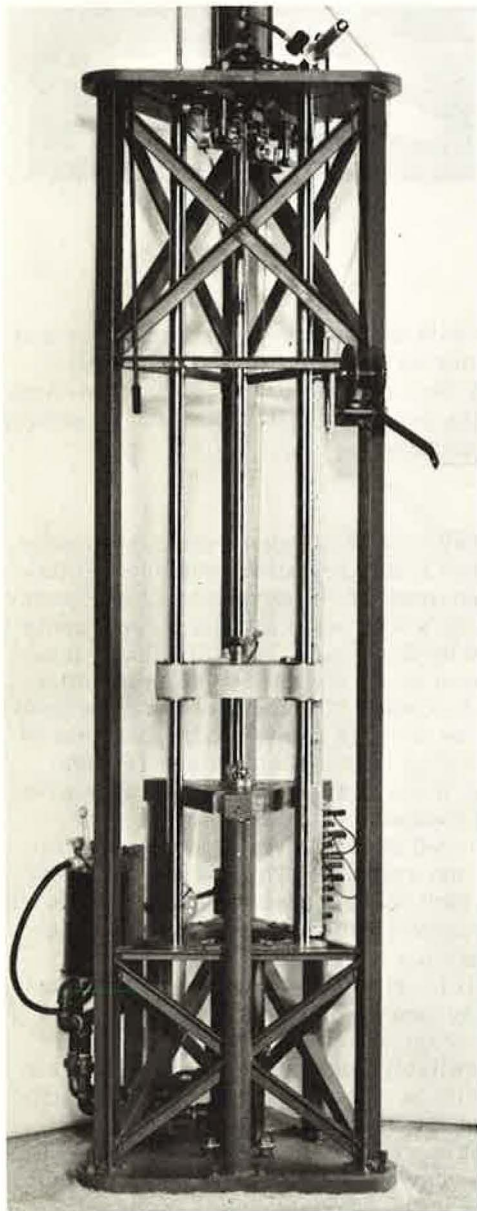


Figure 7.

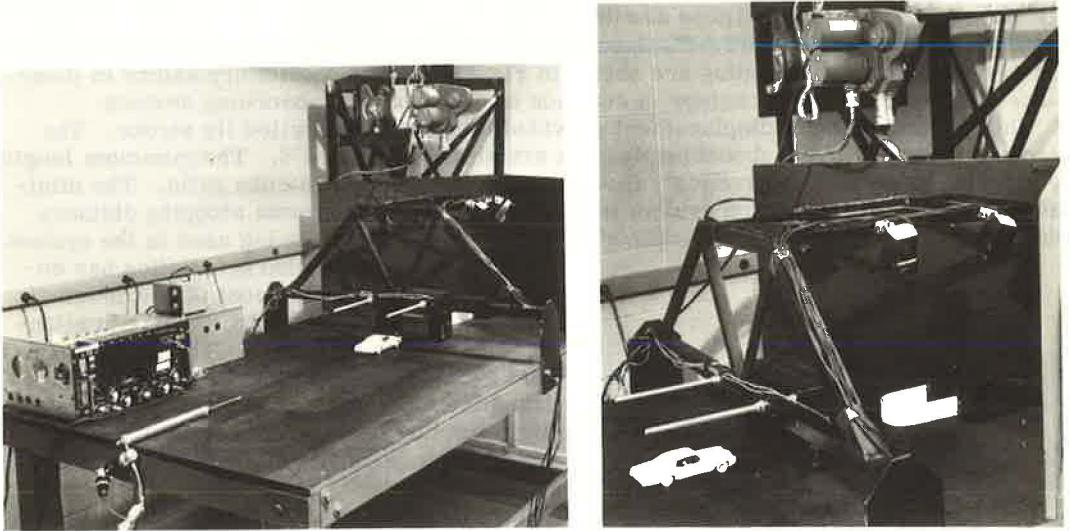


Figure 8.

a record of the velocity of the ram before impact with the energy-absorbing device and the deceleration of the ram as a function of time during the operation of the energy-absorbing device. Additional instrumentation has been developed that gives force-time data. High-speed photography (400 to 3,500 frames per second) is used when necessary to observe the energy-absorbing devices during operation.

Scale-Model Testing

Considerable advancement in the field of highway vehicle attenuators has been made through the use of full-scale tests. However, these tests are quite expensive and time-consuming to set up and run. Much of the data required for the development of highway vehicle attenuator systems can be obtained from tests with scale models. Some scale-model testing has been done of two auto collisions by Emori at UCLA (7). Scale-model tests were also conducted concerning the interaction of autos with the GM redirecting median barrier by Jurkat and Starrett of Stevens Institute of Technology (8). The information obtained from such scale-model tests can be directly related to the behavior of a full-scale prototype by observing appropriate scaling laws and similitude requirements. Scale-modeling has been used extensively in the design of aircraft and is presently being used rather extensively in the field of explosive metal forming.

A scale-model testing facility has been constructed at the University of Denver for the purpose of evaluating highway vehicle attenuation systems. This facility is shown in Figure 8. The facility consists of a table on which scale-model autos are accelerated to desired speeds and directed into scale-model highway buffers. It is equipped with electronic and high-speed photographic instrumentation for recording the crash data. A high-speed camera is mounted above the table (Fig. 8). Other cameras can be mounted on tripods near the table. A velocity measuring system employing light beams and photo transistors is used to measure the velocity of the auto prior to impact with the attenuator. Accelerometers and load cells are available for measuring accelerations and forces in the interaction. The scale-model auto is launched with a pneumatic catapult. The present launching system is capable of launching the auto straight ahead only; future plans call for a launching system that can launch the model with both forward and rotational velocities and also simulate swerving maneuvers prior to impact.

A discussion of the use of dimensional analysis in the scale-modeling of vehicle-attenuator interactions is presented in the Appendix.

REFERENCES

1. Traffic Safety: A National Problem. Eno Foundation for Highway Traffic Control, Saugatuck, Conn., 1967.
2. Viner, J. G., and Tamanini, F. J. The State-of-the-Art of Impact Energy Absorption Barriers. Paper given at the Sixth Annual Louisiana Highway Engineers Conference, Louisiana State University, Baton Rouge, Feb. 1969.
3. Tamanini, F. J., and Viner, J. G. Structural Systems in Support of Highway Safety. Paper given at the ASCE Meeting on Transportation Engineering, Washington, D.C., July 1969.
4. Lacy, J. D., Director, Office of Traffic Operations. Circular Memorandum to Regional Federal Highway Administration and Division Engineers, Dec. 12, 1968.
5. Highway Research Record 222, 1968.
6. Highway Research Record 259, 1969.
7. Emori, R. I., and Link, D. A Model Study of Automobile Collisions. Society of Automotive Engineers, International Automotive Engineering Congress, Detroit, Jan. 13-17, 1969.
8. Jurkat, M. P., and Starrett, J. A. Automobile-Barrier Impact Studies Using Scale Model Vehicles. Highway Research Record 174, 1967, pp. 30-41.
9. Murphy, G. Similitude in Engineering. Ronald Press, New York, 1950.

Appendix

SCALING LAW AND SIMILITUDE REQUIREMENTS FOR TESTING VEHICLE IMPACTS WITH ENERGY-ABSORBING BARRIERS

A physical phenomenon, y , may depend on several independent variables x_1, x_2, \dots, x_n in some unknown manner. In general a functional relationship exists between y and the independent variables that can be expressed as

$$y = f(x_1, x_2, \dots, x_n) \quad (A1)$$

This could be the mathematical expression of a physical law governing the dependence of y on the independent variables, x_1, x_2, \dots, x_n . This physical law is valid regardless of the units of measurement and applies equally well to the model and the prototype. Because the variables in the physical problem (excluding electromagnetic phenomena) can be described in terms of the four basic dimensions of mass, length, time, and temperature, according to Buckingham's pi theorem, the $n + 1$ variables in Eq. A1 can be combined into exactly $n + 1 - k$ dimensionless groups, where k is the number of basic dimensions used to define the n variables. Therefore, Eq. A1 can be put into the dimensionless form

$$\pi_1 = f(\pi_2, \pi_3, \dots, \pi(s)) \quad (A2)$$

The physical law expressed in Eq. A2 is the same for the model and the prototype. If each of the dimensionless variables on the right side of the equation is the same for the prototype and the model, then π_1 will be the same also. This equality between π_1 for the model and for the prototype defines the scaling law for the dependent variable, y . The requirement that the π terms on the right side of the equation be the same for the model as the prototype determines the similitude requirements for the independent variables.

Using the subscripts m and p to refer to model and prototype, the scaling law and similitude requirements are as follows:

Scaling Law:

$$\pi_{1p} = \pi_{1m} \quad (A3)$$

Similitude Requirements:

$$\left. \begin{aligned} \pi_{2p} &= \pi_{2m} \\ \pi_{3p} &= \pi_{3m} \\ &\cdot \\ &\cdot \\ &\cdot \\ \pi_{(s)p} &= \pi_{(s)m} \end{aligned} \right\} \quad (A4)$$

The number of scale factors that may be chosen arbitrarily is equal to the number of basic dimensions in the physical problem. For example, if all the variables in the problem can be expressed in terms of three basic dimensions, i. e., mass, length, and time, three scale factors may be chosen arbitrarily that correspond directly or indirectly to them. The remaining scale factors can be derived in terms of one or more of these factors by using Eqs. A3 and A4.

Example

The use of dimensional analysis to formulate the requirements for the scaling of the interaction between an auto and an energy-absorbing barrier can best be demonstrated by an example. Suppose that an energy-absorbing barrier to be modeled is made of metal and absorbs energy by the deformation of this metal. Let it be assumed that the plastic stress-strain relationship for the metal can be expressed as

$$\sigma = K \epsilon^n$$

where σ is the stress, ϵ is the strain, K is the strain-hardening coefficient, and n is the strain-hardening exponent. It is also assumed for purposes of this example that the auto can be treated as a rigid body.

Denoting the basic dimensions of mass, length, and time by M , L , and T respectively, the variables in the problem are listed below along with their basic dimensions.

	<u>Dependent Variable</u>	<u>Basic Dimensions</u>
a	deceleration of auto during impact	L/T^2
	<u>Independent Variables</u>	
V	velocity of impact	L/T
ω	rotational velocity at impact	$1/T$
I	characteristic polar moment of inertia of auto	ML^2
θ	angle of impact (measured from a coordinate axis)	—
ϕ	yaw angle at impact	—
u	coefficient of friction between tires and road surface	—
γ_i	characteristic dimensions of auto	L
E	modulus of elasticity of barrier material	M/LT^2
ϵ_u	ductility of barrier material (ultimate strain)	—

<u>Independent Variables</u>		<u>Basic Dimensions</u>
L	stroke of barrier	L
σ_u	ultimate strength of barrier	M/LT ²
λ_i	characteristic dimensions of barrier	L
K	strain-hardening coefficient of barrier material	M/LT ²
n	strain-hardening exponent of the barrier material	—
μ	coefficient of friction between the barrier and its support	—
g	acceleration of gravity	L/T ²
M	mass of the vehicle	M
ρ	density of the barrier	M/L ³

There are 19 variables and 3 basic dimensions, so there are 16 independent dimensionless variables required to express the physical relationship. One possible set of dimensionless variables is as follows:

$$\begin{aligned}
 \pi_1 &= aL/V^2 & \pi_9 &= \epsilon_u \\
 \pi_2 &= \omega L/V & \pi_{10} &= K/E \\
 \pi_3 &= I/M\gamma_i^2 & \pi_{11} &= \lambda_i/L \\
 \pi_4 &= \theta & \pi_{12} &= n \\
 \pi_5 &= \phi & \pi_{13} &= \mu \\
 \pi_6 &= u & \pi_{14} &= K/\rho V^2 \\
 \pi_7 &= \gamma_i \omega/V & \pi_{15} &= M/\rho L^3 \\
 \pi_8 &= E/\sigma_u & \pi_{16} &= \frac{gL}{V^2}
 \end{aligned}$$

There are three basic dimensions, so three arbitrary scale factors may be chosen. These are:

$$\begin{aligned}
 n_1 &= \lambda_{im}/\lambda_{ip} \\
 n_2 &= \rho_m/\rho_p \\
 n_3 &= K_m/K_p
 \end{aligned}$$

The scale factors for the remaining variables are derived from these scale factors with the use of the requirement that the dimensionless π terms for the model must equal those for the prototype:

$$\begin{aligned}
 Q_m/Q_p &= \phi_m/\phi_p = \epsilon_{um}/\epsilon_{up} = 1 \\
 \lambda_{im}/\lambda_{ip} &= L_m/L_p = \gamma_{im}/\gamma_{ip} = n_1 \\
 M_m/M_p &= n_1^3 n_2 \\
 I_m/I_p &= n_1^5 n_2 \\
 K_m/K_p &= E_m/E_p = \sigma_{um}/\sigma_{up} = n_3 \\
 a_m/a_p &= n_3/n_1 n_2 \\
 \eta_m/\eta_p &= \mu_m/\mu_p = u_m/u_p = 1
 \end{aligned}$$

$$\begin{aligned}\omega_m/\omega_p &= \frac{1}{n_1} \sqrt{\frac{n_3}{n_2}} \\ V_m/V_p &= \sqrt{\frac{n_3}{n_2}} \\ g_m/g_p &= n_3/n_1 n_2\end{aligned}$$

These scaling factors give the requirements for the dynamic similarity between full-size and model attenuator impacts. Often it is difficult or impossible to scale one or more of the variables properly. In this case gravity cannot be scaled. If the same material is used for the model as for the prototype, n_1 and n_2 are both equal to 1. The similitude requirements then call for the gravity to be $1/n_1$ times as great for the model as for the prototype. If, as in the above example, one or more of the similitude requirements is not satisfied, a distortion is produced such that (9)

$$\pi_{1p} = \delta \pi_{1m} \quad (\text{A5})$$

where δ is the distortion given by

$$\delta = \frac{\pi_{1p}}{\pi_{1m}} = \frac{F(\pi_{2p}, \pi_{3p}, \pi_{4p}, \dots, \pi_{sp})}{F(\pi_{2m}, \pi_{3m}, \pi_{4m}, \dots, \pi_{sm})} \quad (\text{A6})$$

It follows that if only one of the similitude requirements, say π_3 , cannot be satisfied, then

$$\delta = \frac{\pi_{1p}}{\pi_{1m}} = \frac{f(\pi_{2p}, \pi_{3p}, \pi_{4p}, \dots, \pi_{sp})}{f(\pi_{2m}, \pi_{3m}, \pi_{4m}, \dots, \pi_{sm})} \quad (\text{A7})$$

The distortion factor is then given by

$$\delta = \frac{F(\pi_{3p})}{F(\pi_{3m})} \quad (\text{A8})$$

This relationship may be determined experimentally; in some cases it can be determined analytically. It is then used as indicated in Eq. A5 to relate the performance of the distorted model to that of the prototype.

Dragnet Vehicle Arresting System

GORDON G. HAYES, T. J. HIRSCH, and DON L. IVEY,
Texas Transportation Institute, Texas A&M University

The "dragnet" vehicle arresting system consists of a net made of steel cables attached at each end to Metal Bender energy-absorbing devices. The system was subjected to six full-scale automobile crash tests to evaluate its performance in stopping a speeding vehicle over a relatively short distance with acceptable deceleration levels. The decelerations encountered were significantly lower than those produced by rigid barriers, and could have been reduced even more by the use of less restraining force on the net, resulting in longer stopping distances. Time-displacement and deceleration data (and observation of damage) from the test series, along with the predictability of system performance in specified situations, indicate that practical application of the arresting system at such locations as dead ends of roads, ferry landings, and highway medians at bridge overpasses is feasible.

●VEHICLE crash testing contributes significantly to the development of new concepts and devices to increase highway safety. However, it is also a valuable tool for determining the applicability of existing devices to highway safety problems.

One existing device that was subjected to full-scale crash testing by the Texas Transportation Institute is the "dragnet" vehicle arresting system developed by Van Zelm Associates, Inc., of Providence, Rhode Island. Six tests were conducted under a contract with the Bureau of Public Roads as part of their program on Structural Systems in Support of Highway Safety (4S Program).

The system, which consists of a steel net attached at each end to Metal Bender energy-absorbing devices, has been used on "drag strip" raceways and, in a modified form, for aircraft arrests, but prior to this test program the dragnet system has not been widely applied to suitable locations on the public roads. This may be due to the lack of independent analysis of the system's effectiveness in such applications.

DESCRIPTION OF ARRESTING SYSTEM

This system consists of a net made of steel cables attached at each end to Metal Bender energy-absorbing devices as shown in Figures 1 and 2. The Metal Benders, which are supported on rigid steel posts, are steel boxes containing a series of rollers around which the metal tape is bent back and forth as it is pulled through the case. Each end of the net is attached to one end of the metal tape extending from a Metal Bender. The Metal Benders are designed so that a specified force will be necessary to pull the metal tape through the case. This force is relatively independent of velocity and environmental conditions and depends on the size of the tape used. By varying tape size, a number of different tape forces are available.

TEST PROGRAM

Six vehicle crash tests of the dragnet arresting system were conducted during the period from December 19, 1967, to November 21, 1968. A summary of this testing

program is given in Table 1. Both compact and full-sized vehicles were directed into the system. Tests A through D employed Metal Benders with 25,000-lb tape loads. These tape loads were reduced to 12,500 lb for Tests E and F.

Each test was recorded using high-speed motion picture cameras. The film was analyzed to give detailed time-displacement data. Lower speed motion picture cameras were placed at selected points to provide a qualitative record of the test in progress. Still photographs of the vehicle before and after each test and photographs of various details of the arresting system were obtained.

Accelerometer transducers were attached to the frames of the vehicles to determine deceleration levels during each test. Maximum decelerations under specified filtering techniques were determined



Figure 1. Metal Bender with 25,000-lb tape attached to net.

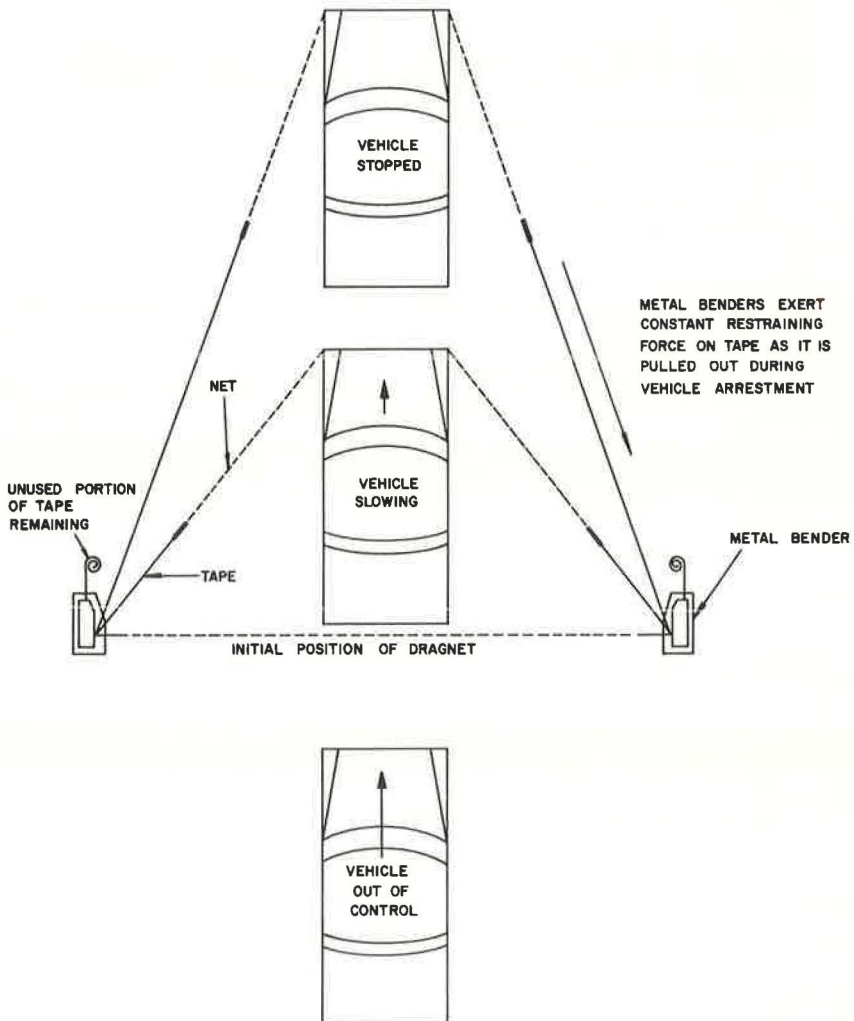


Figure 2. Idealized function of dragnet arresting system.

from these accelerometer traces, while average decelerations were calculated on the basis of initial speed and stopping distance.

An Alderson articulated anthropometric dummy weighing 161 pounds was used to simulate a human driver in each test. A seat belt securing the dummy was equipped with strain gages that permitted the measurement of seat belt force.

Test A

A Renault Dauphine weighing 1,460 pounds was directed head-on into the dragnet at a speed of 42 mph. The tape force for each Metal Bender was 25,000 lb. All components of the system performed as designed and the vehicle was stopped after penetrating 10.2 ft. Stopping distance is defined as the distance the center of gravity of the vehicle travels after the vehicle contacts the net. The Metal Bender strap pullout accounted for 63 percent of the vehicle's initial kinetic energy of 87.1 kip-ft. The remaining energy was expended in stretching the net, crushing the vehicle, and increasing the vehicle's potential energy due to raising the center of gravity. The amount expended in increasing gravitational potential energy was only about 1 kip-ft.

The damage to the front of the vehicle was severe (Fig. 3). The maximum longitudinal deceleration was 16 g. The average deceleration was 5.8 g over 0.25 second.

Test B

A 4,300-lb Mercury sedan traveling at 60 mph was directed head-on into the arresting system. The dragnet, which was equipped with 25,000-lb tape tension Metal Benders, performed as designed. The vehicle was brought to a stop in 19.4 ft and tape pullout expended 58 percent of the vehicle's energy. The front of the vehicle was pulled down to the ground, which caused some frictional energy losses. The change in potential energy due to the elevation of the center of gravity was estimated to be about 17 kip-ft, or 3.3 percent of the initial energy.

The damage to the front of the vehicle, shown in Figure 4, includes a downward bending of the front of the vehicle's frame. This was due to the net applying pressure to the lower portion of the vehicle's front end. The maximum significant deceleration was 16 g, and the average deceleration was 6.1 g.

Test C

A 1,620-lb Volkswagen traveling at 48 mph entered the arresting system at an angle of 30 deg to the perpendicular to the net. All subsequent angle tests will be defined on this basis. The vehicle was stopped in 13.8 ft, and pulled a total of 3.4 ft of tape out of



Figure 3. Vehicle and dragnet after Test A.



Figure 4. Vehicle and left Metal Bender after Test B.



Figure 5. Vehicle after Test C.

the 25,000-lb Metal Benders. This tape pullout consumed 70 percent of the vehicle's kinetic energy. The estimated energy necessary to impart a horizontal rotation, or spin, to the vehicle and to elevate its center of gravity was about 3 kip-ft. These energy levels are defined at the time during the test when the tapes stop pulling out of the benders. The average deceleration level was 5.5 g, while the maximum deceleration was about 13 g. The vehicle damage as shown in Figure 5 was moderate.

Test D

In Test D a 4,520-lb Oldsmobile sedan traveling at 54 mph impacted the net on an initial trajectory of 30 deg. The high-speed films show a maximum travel of 23.5 ft after impact. The 25,000-lb Metal Benders allowed 8.6 ft of metal tape to be pulled through, accounting for 50 percent of the initial

kinetic energy. When the maximum tape pullout had occurred, the vehicle was estimated to have 36 kip-ft of rotational energy and 11 kip-ft of gravitational potential energy. The net entrapped only the lower portion of the front of the vehicle. As the front pulled down below the vehicle center of gravity, the unbalanced inertia force resulted in the vehicle's rotating about the restrained point (Fig. 6). The vehicle was completely off the ground and the rear end went over and outside of the restraining net after the tapes had stopped pulling out. When the vehicle fell back to the ground, it came very close to rolling. The average and maximum significant longitudinal decelerations were 4.1 and 8g respectively.

Test E

Test E was similar to Test B in that a heavy car, a 3,760-lb Dodge sedan, was directed head-on into the dragnet at a velocity of 56 mph. However, in this and the following test the Metal Bender tape load was decreased to 12,500 lb and the net was raised about 4 in. off the ground to better entrap the front of the vehicles.

The vehicle was stopped in 26.3 ft and pulled out a total of 30.7 ft of tape, which is equivalent to 384 kip-ft, or 96 percent of the vehicle's kinetic energy. The vehicle had

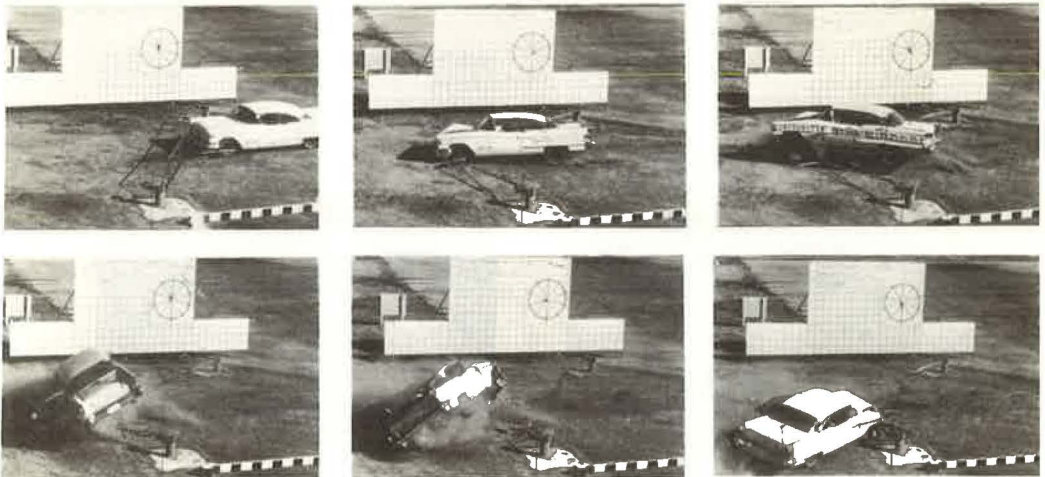


Figure 6. Sequential photographs of Test D showing behavior of net during arrestment.

no significant rotational energy at maximum penetration, but had gained about 7 kip-ft of gravitational potential energy.

The vehicle damage was minor (Fig. 7), as would be expected since the maximum deceleration was only 7.0 g, and the average deceleration was 4.0 g.

Test F

As the final test in this series, a 3,880-lb Ford sedan traveling at 62 mph collided with the dragnet at an impact angle of 30 deg. As in the previous test, 12,500-lb Metal Bender tapes were used.

The tape on the right side was expended and pulled free of the Metal Bender before the vehicle had been brought to a stop (Fig. 8). The system performed as designed up to the point of tape pullout. The net, which was still attached to one Metal Bender, caused the vehicle to spin through an angle of about 120 deg after pulling out the right tape before coming to rest.

The total tape pullout when the right tape pulled free was 32.9 ft, which accounts for 89 percent of the kinetic energy lost up to that point. The high-speed films indicate that the vehicle had lost about 91 percent of its initial energy at this point and that the speed was down to about 17 mph.

The total tape pullout of 38.5 ft at full stop accounts for 94 percent of the vehicle's initial energy. Comparisons of actual and theoretical values are made up to the point of tape expenditure.

The deceleration levels of 5.0 g (maximum) and 2.4 g (average) are tolerable to restrained humans (1).

RESULTS

The complete test series conducted on the Van Zelm dragnet is summarized in Table 1. The vehicles used ranged in weight from 1,460 to 4,520 lb. All test vehicles impacted the dragnet at its center. Tests A, B, and E were head-on tests, while Tests C, D, and F were 30-deg angle tests. This means that the initial trajectory of the vehicle made an angle of 30 deg with a perpendicular to the original position of the dragnet.

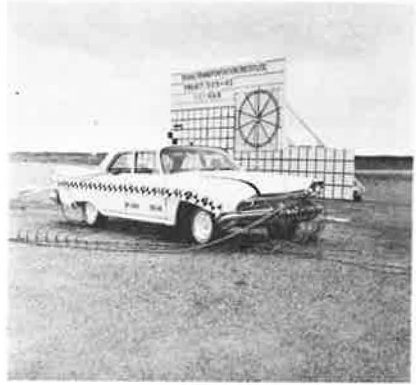


Figure 7. Vehicle after Test E.

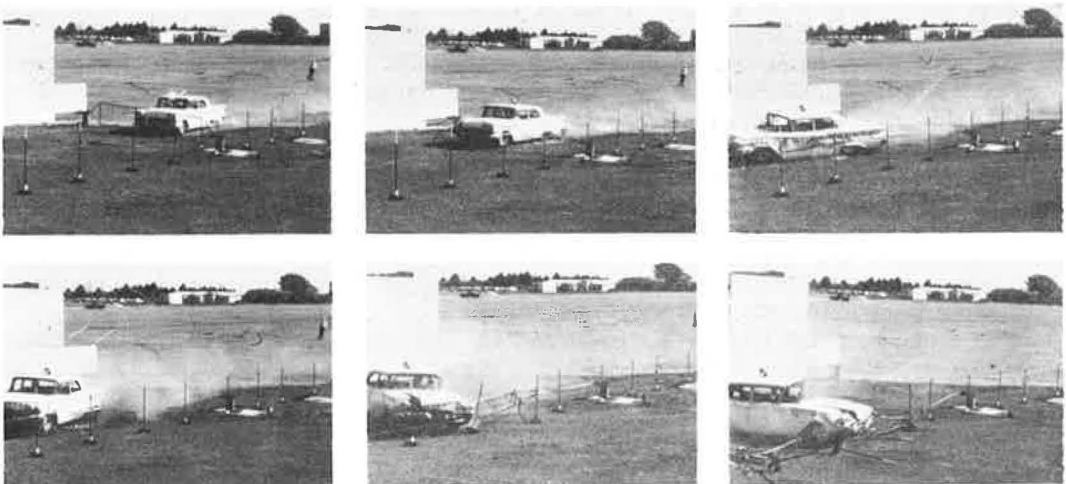


Figure 8. Sequential photographs of Test F.

TABLE 1
SUMMARY OF TEST RESULTS

Factor	Test					
	A	B	C	D	E	F
Angle of impact	Head-on	Head-on	30 deg	30 deg	Head-on	30 deg
Vehicle weight (lb)	1,460	4,300	1,620	4,520	3,760	3,880
Vehicle speed (mph)	42	60	48	54	56	62
Metal Bender tape load (kip)	25	25	25	25	12.5	12.5
Vehicle deformation (ft)	1.8	1.0	0.9	1.5	0.3	0.5
Vehicle stopping distance (ft)	10.2	19.4	13.8	23.2	26.3	29.5 ^a
Total Metal Bender tape pullout (ft)	2.2	11.8	3.4	8.6	30.7	32.9 ^a
Energy absorbed by	54.8	296	86	214	384	411 ^a
Metal Bender (kip-ft)	(63 %)	(58 %)	(70 %)	(50 %)	(96 %)	(89 %)
Maximum significant deceleration (g), electromechanical curves	16	16	13	8	7	5
Average deceleration (g), film, $V^2/2gX_{max}$	5.8	6.1	5.5	4.1	4.0	2.4 ^a
Duration of impact (seconds)	0.25	0.39	0.29	0.48	0.67	0.49

^aUp to point tape expended.

Tapes producing a 25-kip pull were used in Tests A through D, while in Tests E and F this tape force was reduced to 12.5 kips.

The energy absorbed by the Metal Benders ranged from 50 percent to 70 percent of the vehicle's initial kinetic energy for the first four tests, which used the 25-kip tape loads. In Tests E and F the percent of energy absorbed by the Metal Benders ranged from 89 percent to 96 percent. There are several reasons for this difference. At the end of Metal Bender tape pullout, which corresponds approximately to zero longitudinal velocity, significant amounts of energy may remain in the form of gravitational potential energy and rotational kinetic energy. In most impacts there is some gravitational potential energy gain caused by the tendency of the net to pull the vehicle down in front and the tendency for the rear end to rise. This results in an increase in the elevation of the vehicle's center of gravity. In the case of angle tests, there may be a significant amount of horizontal rotational energy present, equal to half the product of the vehicle mass moment of inertia (about the vertical axis through the vehicle's center of gravity) times the square of the vehicle's angular velocity about this axis. Also present may be transverse rotational energy, which is defined in the same way as the horizontal rotational energy except that the mass moment of inertia and angular velocity is about the longitudinal vehicle axis. Other energy expenditures may be accounted for by the axial strain energy that goes into the cable and tapes, the vehicle deformation, and frictional losses such as contact of rigid portions of the vehicle with the ground. This last energy expenditure was prevalent in Test B. It can be concluded, at least within the range of tape forces tested, that the lower the tape force the greater the percentage of energy dissipated in the Metal Benders. If the extreme example of a tape with infinite load capacity is considered, almost all of the kinetic energy of the vehicle would be expended in vehicle deformation, rolling, etc.

A convenient way of indicating the relative desirability of dragnet arrestments is to compare the deceleration levels determined by these tests with the decelerations that would be encountered during a collision with a rigid barrier. The attenuation index is defined as the ratio of decelerations during an attenuated arrestment by dragnet, for example, with those estimated decelerations during a rigid barrier impact (2). Both maximum and average attenuation indexes (AI_{max} and AI_{avg}), which compare maximum and average deceleration levels, are given in Table 2.

Tests E and F, using 12,500-lb Metal Benders, have smaller attenuation indexes than the first four tests. This is the obvious result of cutting the stopping force in half. This reduction in stopping force significantly reduces the vehicle damage. The relatively large energy differences between tape energy and initial kinetic energy in Tests A through D are the result of large energy expenditures on vehicle deformation.

In the Appendix is a theoretical treatment that algebraically relates vehicle weight, velocity, tape force, and stopping distance. The error induced by considering the vehicle

TABLE 2
COMPARISON OF VAN ZELM DRAGNET PERFORMANCE WITH RIGID BARRIER IMPACT

Factor	Test					
	A	B	C	D	E	F
Metal Bender tape load (kip)	25	25	25	25	12.5	12.5
Vehicle weight (lb)	1,460	4,300	1,620	4,520	3,760	3,880
Vehicle velocity (mph)	42	60	48	54	56	62
Maximum deceleration (G_{max})						
Dragnet ^a	16	16	13	8	7.0	5.0
Rigid barrier ^b	37.8	54.0	43.2	48.6	50.4	55.8
Average deceleration (G_{avg})						
Dragnet ^c	5.8	6.1	5.5	4.1	4.0	2.4
Rigid barrier ^d	24.1	34.4	27.6	31.0	32.1	35.6
Attenuation index						
$AI_{max} = \frac{G_{max} \text{ Dragnet}}{G_{max} \text{ Rigid}}$	0.42	0.30	0.30	0.17	0.14	0.09
$AI_{avg} = \frac{G_{avg} \text{ Dragnet}}{G_{avg} \text{ Rigid}}$	0.24	0.18	0.20	0.13	0.12	0.07

^a G_{max} Dragnet is from frame accelerometer data.

^b G_{max} Rigid = 0.9 (vehicle velocity in mph) (2).

^c G_{avg} Dragnet = $\frac{V^2}{2gX_{max}}$ from film data.

^d G_{avg} Rigid = 0.574 (vehicle velocity in mph) (2).

to have no finite width is approximately compensated for by the fact that after impact the "spreaders" at the ends of the net buckle, increasing the effective length of the net. Because the main net cables loop over and under the front of the vehicles and the vehicles are deformed differently, some inaccuracy is expected, especially in arrestments with short stopping distances. It is also assumed in the calculations that the vehicle continues along its original path during arrestments, which is only a rough approximation in angled or noncentric hits.

Figure 9 is a plot of dragnet force on the vehicles against distance traveled after contact. The data used for this plot are taken from the theoretical calculations in the Appendix.

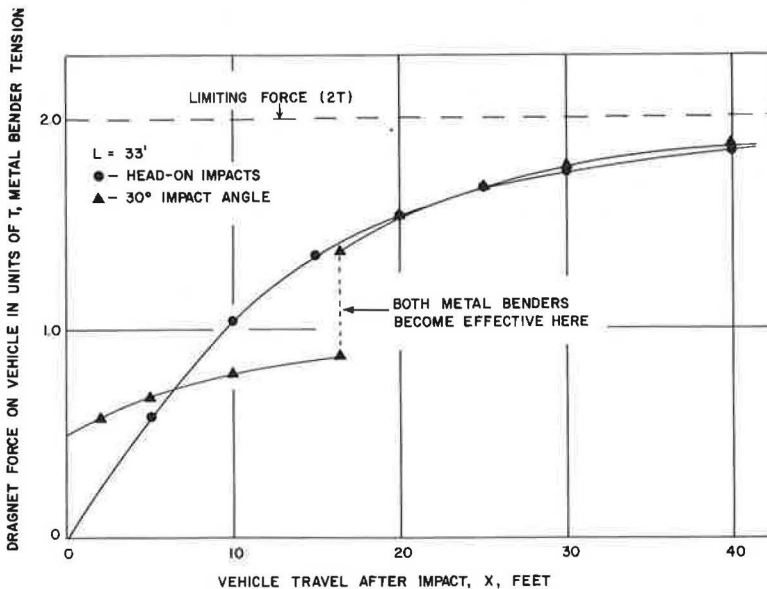


Figure 9. Theoretical stopping force-displacement curves for centric impacts.

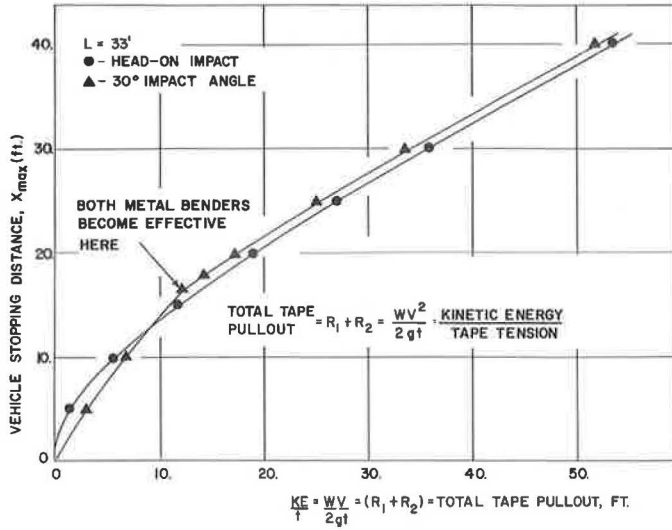


Figure 10. Stopping distance vs. total tape pullout.

From the theoretical treatment, a plot of total Metal Bender tape pullout against X_{max} , the theoretical stopping distance, was made for head-on and 30-deg angled impacts. Neglecting other energy-dissipation modes, the initial vehicle kinetic energy divided by the Metal Bender tape tension should equal the total tape pullout. By taking the initial velocity, determined from the high-speed films, and calculating initial kinetic energy, and by knowing the Metal Bender tape tensions, we can calculate the theoretical total tape pullout. Using this value and Figure 10, we can determine theoretical stopping distance. The theoretical stopping distances so determined are compared with actual stopping distances from the high-speed film data in Table 3. In this comparison, the measured stopping distance is the measured stopping distance of the vehicle's center of gravity minus the vehicle's deformation. (This is the distance traveled by the vehicle's front end after contacting the net.)

Again, the percentage difference between actual and theoretical values is greater for short stopping distances (high Metal Bender tensions). Examination of the high-speed films indicates that in Test C the combination of the low, narrow front end of the vehicle and the collapse of the end net spreaders, which occurred in every test, delays application of the main stopping force until the vehicle has traveled about 4 ft beyond initial contact. This is a considerable portion of the total stopping distance, and explains the large difference between measured and calculated stopping distance. For this vehicle's initial energy, the calculated total tape pullout is 4.9 ft. This compares favorably with the actual measured tape pullout of 3.4 ft.

TABLE 3
COMPARISON OF COMPUTED STOPPING DISTANCES WITH MEASURED STOPPING DISTANCES

Stopping Distance	Test					F ^a
	A	B	C	D	E	
$(X_{max})_M$ (ft) ^b	8.4	18.4	12.9	22.0	26.0	29.0
$(X_{max})_C$ (ft) ^c	7.8	21.0	7.6	20.2	27.7	29.5
$[(X_{max})_C - (X_{max})_M]$ (ft)	-0.6	+2.6	-5.3	-1.8	+1.7	+0.5

^aCalculated up to point metal tape was expended.

^bMeasured stopping distance from film minus vehicle deformation.

^cCalculated stopping distance from initial vehicle velocity and theoretical treatment in Appendix.

CONCLUSIONS

The Van Zelm dragnet vehicle arresting system performed basically as designed in all tests. The performance of the system was very good in four of the six tests. In Test D the dragnet was engaged too low on the front of the vehicle, which resulted in the vehicle's rear end vaulting the net after most of the longitudinal deceleration had occurred. In Test F the performance of the dragnet system was ideal until one of the tapes ran out. Had this tape been long enough to continue applying load until the vehicle was completely stopped, the performance probably would have been excellent. Deceleration levels were reduced to a small fraction of those that would be expected in rigid barrier impacts. Increasing design tape load results in shortening the stopping distance, increasing the deceleration level and increasing vehicle damage. For any given application of the dragnet system, the longer the allowable stopping distance, the more desirable the deceleration characteristics of the system because a smaller tape load can be used.

The height of the net was shown to be an important factor in the performance of the system. The net should be positioned so that it completely entraps the front of the entering vehicle. If it is too low, a less desirable performance may be expected, as was found in Test D. Good performance was found when the lower main cable of the net was positioned 4 in. above the ground.

No permanent damage was sustained by the dragnet system during any of these tests. All major components were reusable except for the expendable metal tapes. The system can be applied to a variety of situations by varying the Metal Bender tape tension, the tape length, and the geometry of the installation. A variety of Metal Bender tape tensions are available from Van Zelm Associates.

This series of tests has shown that reasonably accurate predictions of vehicle stopping distance and deceleration levels can be obtained using the equations developed in the Appendix.

RECOMMENDATIONS

The dragnet vehicle arresting system is an effective, practical, and economical system for safely stopping vehicles that are out of control at certain highway sites. Some obvious locations for its employment are

1. Across highway medians between double bridges,
2. At "dead ends" of highways or roads,
3. At ferry landings or drawbridges, and
4. In front of certain rigid obstacles in highway rights-of-way.

It is recommended that the height of the arresting net be increased to approximately 4 ft. The net used in these tests was 3 ft high, and in several tests (notably Test D) it failed to completely entrap the vehicle's front end. It is desirable that the upper net cable clear the top of the vehicle hood in order to more securely entrap the vehicle.

The lowest Metal Bender tension force compatible with the available stopping distance should be selected. In general, Metal Bender tension forces of 12,500 lb or less are recommended. The behavior of these dragnet systems can be predicted very well with the mathematical analysis presented in the Appendix.

REFERENCES

1. Damon, A., Stoudt, H. W., and McFarland, R. A. *The Human Body in Equipment Design*. Harvard University Press, Cambridge, Mass., 1966.
2. Emori, Richard I. Analytical Approach to Automobile Collisions. SAE Paper 680016, Engineering Congress, Detroit, Jan. 8, 1968.

Appendix

SIMPLIFIED THEORETICAL ANALYSIS

Relatively simple equations will be developed here that will aid in selecting a desirable Metal Bender tape tension force (T) and length (R_{\max}) in order to stop a vehicle of given weight (W) and speed (V).

Van Zelm now has available metal tapes and Metal Benders (sometimes called "tor-ture chambers") that provide tape tension forces (T) of 2,500 lb, 4,000 lb, 12,500 lb, 18,750 lb, and 25,000 lb. Two of the 4,000-lb Metal Benders can be stacked on top of each other to provide a tape tension force of 8,000 lb.

For these tape tension forces, we can compute the minimum required length of tape (R), the stopping distance required (X_{\max}), and the maximum and average g forces on the vehicle as follows:

$$\text{Kinetic Energy of Vehicle} = \frac{WV^2}{2g}$$

Assuming all energy is absorbed by Metal Bender tape,

$$2TR_{\max} = \frac{WV^2}{2g}$$

the maximum tape run-out is then

$$R_{\max} = \frac{WV^2}{4Tg} \text{ and } R_{\max} = R_{1\max} = R_{2\max} \quad (1)$$

since the system is symmetrical in this case. From Figure 11,

$$X = \sqrt{\left(R + \frac{L}{2}\right)^2 - \left(\frac{L}{2}\right)^2} \quad (2a)$$

$$X_{\max} = \sqrt{R_{\max}^2 + R_{\max} L} \quad (2b)$$

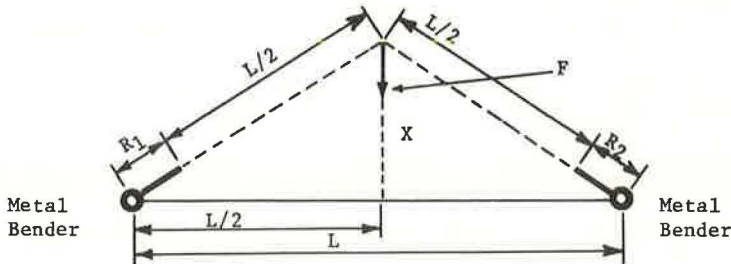


Figure 11. Diagram for analysis of Van Zelm Metal Bender dragnet system head-on centric vehicle collision. L = length of net, ft; T = Metal Bender tape tension force, lb; $R = R_1 = R_2$ = run-out of Metal Bender tape (assuming all energy is absorbed by tape), ft; X = travel distance of vehicle after engaging net, ft; X_{\max} = stopping distance, ft; F = stopping force component on vehicle, lb; W = weight of vehicle, lb; V = initial velocity of vehicle, ft/sec; and g = acceleration due to gravity, 32.2 ft/sec².

If the stopping force component on the vehicle is

$$F = 2T \left(\frac{X}{R + \frac{L}{2}} \right) \quad (3a)$$

then the maximum vehicle stopping force for head-on collisions would be

$$F_{\max} = 2T \left(\frac{X_{\max}}{R_{\max} + \frac{L}{2}} \right) \quad (3b)$$

The maximum G force on the vehicle is

$$G_{\max} = \frac{F_{\max}}{W} \quad (4)$$

The average G force on the vehicle would be

$$G_{\text{avg}} = \frac{V^2}{2gX_{\max}} \quad (5)$$

From Eq. 2a,

$$R = \frac{1}{2} \sqrt{L^2 + 4X^2} - \frac{L}{2}$$

so that

$$F = 2T \left[\frac{1}{\sqrt{\left(\frac{L}{2X}\right)^2 + 1}} \right] \quad (6)$$

The analysis for angled impacts resulted in the following equation of stopping distance for 30-deg angles:

$$X_{\max} = \sqrt{\left(\frac{WV^2}{4gT}\right) \left(\frac{WV^2}{4gT} + L\right)} \quad (7)$$

More details on the analysis and a design example are found in "Dragnet Vehicle Arresting System," Technical Memorandum 505-4, Texas Transportation Institute, Texas A&M University, which is available through the authors.

Feasibility of Lightweight Cellular Concrete for Vehicle Crash Cushions

DON L. IVEY, EUGENE BUTH, and T. J. HIRSCH,
Texas Transportation Institute, Texas A&M University

Three vehicle crash tests of lightweight cellular concrete crash cushions are reported, along with proposed procedures for cast-in-place and pre-cast construction of these devices. This crash cushion, composed of vermiculite concrete, lightweight welded wire fabric, and cylindrical cardboard forms, is designed to protect motorists from collisions with rigid obstacles located along the roadway. The crash cushion has proved crash-worthy under head-on test conditions.

•CELLULAR concrete structures have been proposed as vehicle deceleration devices in a recent feasibility study by Cornell Aeronautical Laboratories (1). Three vehicle crash tests have been conducted on a lightweight cellular concrete crash cushion (designed by personnel of the Texas Transportation Institute) with very favorable results. The crash cushion is composed of vermiculite concrete with hollow cardboard tubes (23 in. in diameter) spaced throughout to provide the necessary voids. Lightweight welded wire fabric is used as reinforcement for the vermiculite. The first concrete crash cushion constructed is shown in Figures 1 and 2.

The concrete used for the crash cushions in this study was composed of cement, water, and a commercial grade of vermiculite. This vermiculite aggregate was very uniform in gradation. Vermiculite is a kiln-expanded mica. Since mica is a rock composed of many thin layers, it is subject to high expansion, leaving spaces between these layers. The average size particle is approximately a $\frac{1}{8}$ -in. cube. On close examination, a single cubical particle looks like a tiny accordion. These small cubes can be compressed to a flat particle by slight pressure. The extreme light weight (per bulk volume) of this aggregate in combination with a high degree of air entrainment produces a very lightweight, low-strength concrete.

MATERIALS AND CONSTRUCTION

A 1:7 mixture of vermiculite concrete was used in all three crash cushions. Coarse vermiculite aggregate and type III cement were used in the cushions for

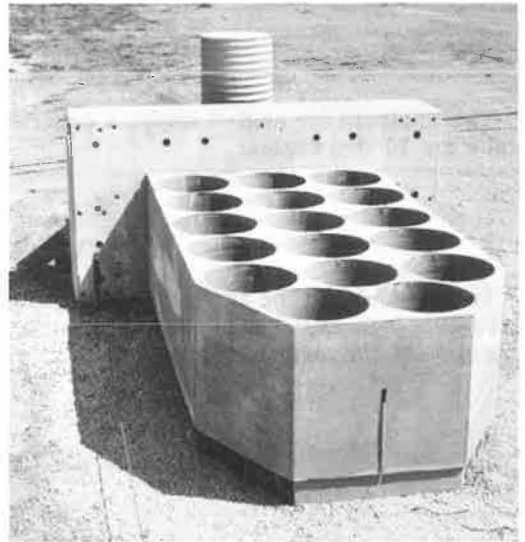


Figure 1. Prototype of concrete crash cushion.

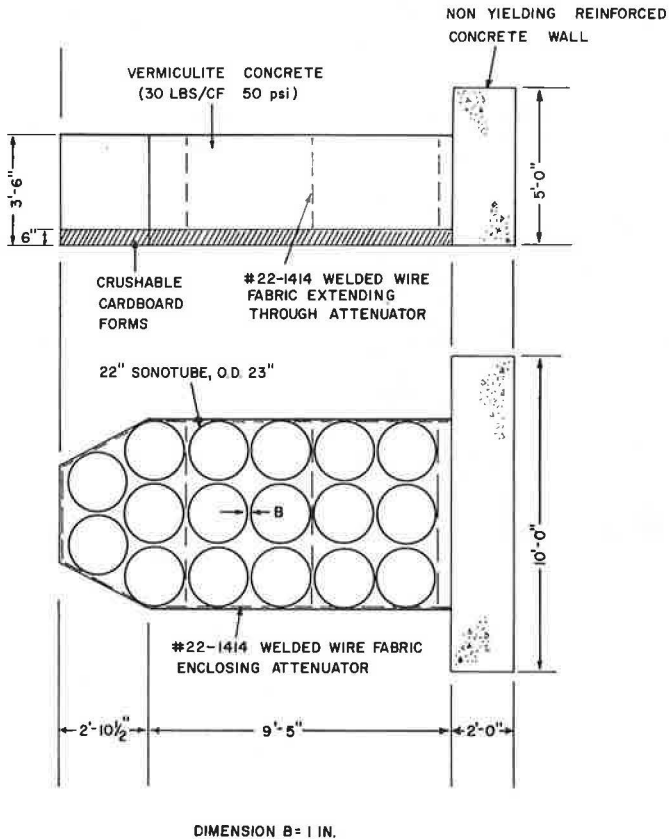


Figure 2. Concrete crash cushion, Test A.

Tests A and B. Welded wire fabric (24-1414) reinforcement was placed longitudinally in each side wall and transversely between each row of sonotubes in the Test A cushion. In the Test B cushion, a layer of this wire fabric was also placed in the top and bottom surfaces. Mixture proportions and properties of the concrete are given in Table 1. Folding cardboard carton forms were used as the bottom form with reinforced $\frac{3}{4}$ -in. plywood sheets used for the side forms. In Tests A and B, the cardboard carton forms

TABLE 1
MIXTURE PROPORTIONS AND PROPERTIES OF VERMICULITE CONCRETE

Test	Aggregate	Cement	Water	Wet Unit Weight	Dry Unit Weight	Compressive Strength
A	121.3 lb/cu yd 20.2 cu ft/cu yd	272 lb/cu yd 2.9 sacks/cu yd	607 lb/cu yd 72.9 gal/cu yd 25.1 gal/sack	37 lb/cu ft	32 lb/cu ft at 12 days	50 psi at 12 days
B	140 lb/cu yd 23.4 cu ft/cu yd	312 lb/cu yd 3.34 sacks/cu yd	629 lb/cu yd 75.5 gal/cu yd 22.6 gal/sack	40 lb/cu ft	32 lb/cu ft at 18 days	71 psi at 13 days
C	150 lb/cu yd 23.0 cu ft/cu yd	305 lb/cu yd 3.24 sacks/cu yd	645 lb/cu yd 77.4 gal/cu yd 23.9 gal/sack	41 lb/cu ft average	21 lb/cu ft at 30 days	57 psi at 30 days



Figure 3. Precast vermiculite module.

remained in place and supported the cushion 6 in. above ground level when installed at the test site. The sonotube spacing was maintained with small wooden blocks.

The cushion for Test A was cast as a single unit, then transported to the test site and installed. The Test B cushion was cast in place at the test site. Precast modules were used in constructing the cushion for Test C. One of the three-tube modules is shown in Figure 3. The welded wire fabric was placed in all four outside walls of the forms. Using a new fast-setting cement developed by the Portland Cement Association, the forms were removed in less than 2 hours after casting. This cement was furnished by the Lone Star Cement Corporation and is still in the experimental stage.

TEST PROGRAM

Three full-scale vehicle crash tests of the lightweight cellular concrete crash cushion have been conducted. Electronic accelerometers and an Impact-O-Graph were used in each test to record decelerations. High-speed cameras (500 frames per second) recorded the crash, and analysis of the film gives vehicle displacement and velocity with respect to time. Rough estimates of

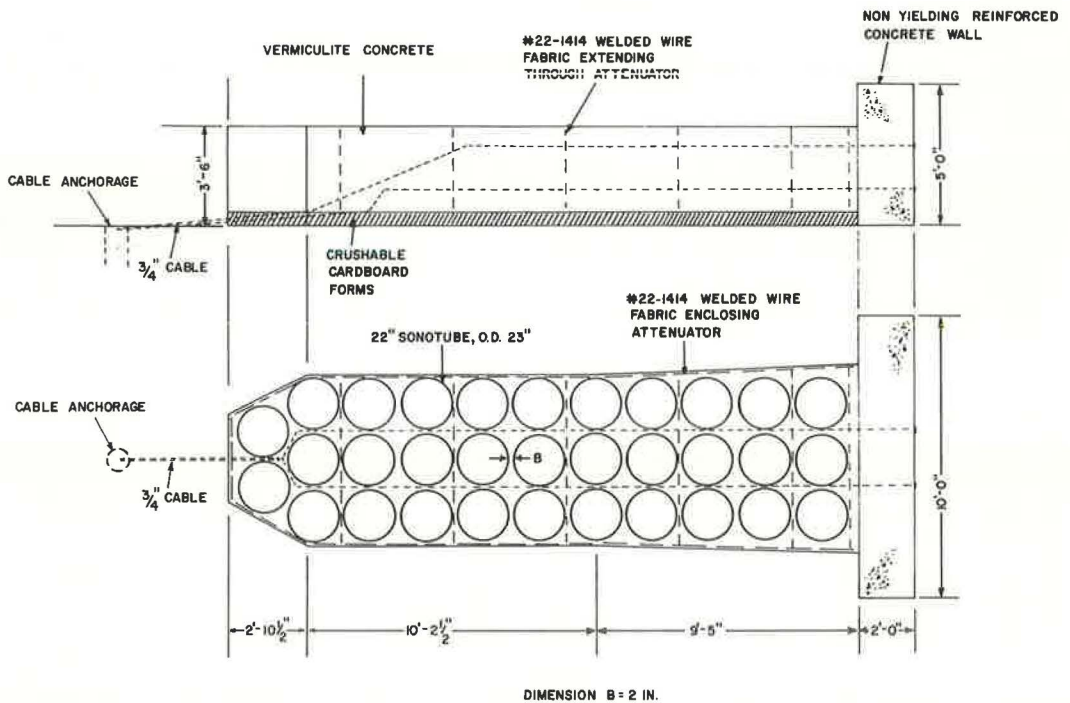


Figure 4. Concrete crash cushion, Test B.

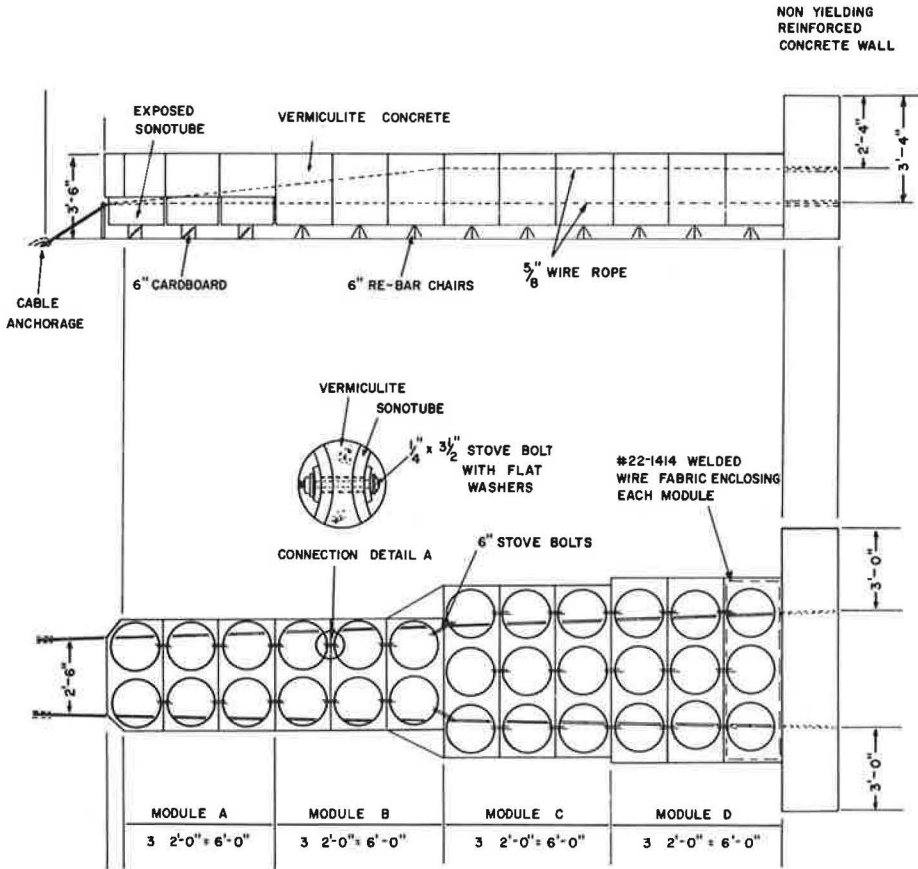


Figure 5. Concrete crash cushion, Test C.

deceleration over distances of several feet can also be achieved by analysis of the photographs of the vehicle and crash cushion and sequential photographs of the test in progress are included.

Crash Tests

In Test A, only half of the proposed full-sized crash cushion was fabricated. The first 12 ft of the cushion, shown in Figure 1, was subjected to a low-speed test (41 mph) by a 3,650-lb vehicle. In Test B, a full-sized crash cushion (24 ft in length) was cast in place (Fig. 4). In this test, a 3,200-lb vehicle impacted the cushion at a velocity of 59 mph. In Test C, the precast modular construction technique was used and the barrier was put together in the field using three-tube and two-tube modules. The design of this cushion is shown in Figure 5. A 4,560-lb vehicle traveling 64 mph impacted this crash cushion head on. For comparison purposes, the test of a 3,270-lb vehicle



Figure 6. Crash Test D (immovable wall).

TABLE 2
SUMMARY OF TEST DATA

Factor	Test			
	A	B	C	D (Rigid Wall)
Vehicle year, make, and model	1956 Pontiac 4-door	1963 Dodge 4-door	1958 Oldsmobile 2-door	1963 Plymouth 4-door
Vehicle weight (W), lb	3,650	3,200	4,560	3,270
Vehicle velocity (V), fps	60.3	86.2	93.3	78.3
mph	41.1	58.8	63.6	53.3
Stopping distance (D), ft	9.0	11.2	21.4	3.82
Maximum deceleration (longitudinal), g	10.5 ^a	20.5 ^a	10.4 ^a	35 ^a
Average deceleration (longitudinal), g	5.1 ^a 6.3 ^b	6.6 ^a 10.3 ^b	6.5 ^a 6.3 ^b	25 ^b
Attenuation index ^c				
AI(max) = $\frac{G(\text{maximum test})}{G(\text{maximum rigid})}$	0.29	0.39	0.18	0.73
AI(avg) = $\frac{G(\text{average test})}{G(\text{average rigid})}$	0.27	0.31	0.17	0.82

^aElectronic accelerometer; data on Test B not reliable due to zero shift.
^bCalculated from stopping distance.
^cG (maximum rigid) = 0.9V, G (average rigid) = 0.574V, V in mph (2).

traveling 53 mph and impacting a rigid wall is included. This test is designated D and is shown in Figure 6.

These four head-on tests are summarized in Table 2. In Test A (Fig. 7), the 1956 Pontiac was stopped in 9 ft with an average barrier force of 23,000 lb. The average deceleration was 6.3 g, which is considered an acceptable level. Test B illustrated the

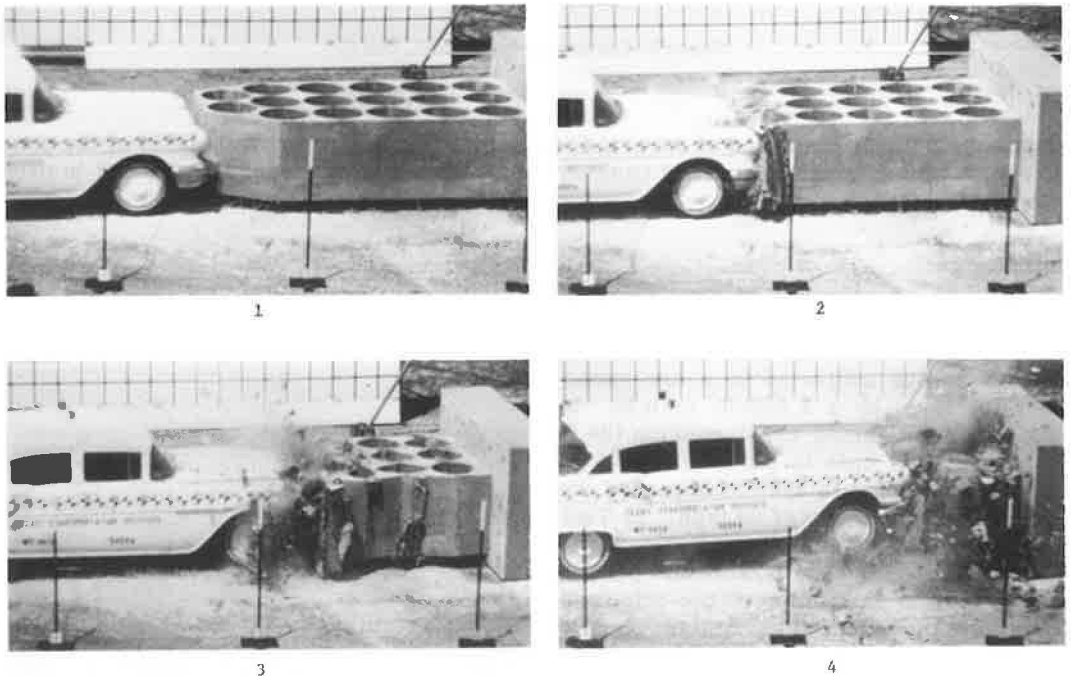


Figure 7. Sequential photographs of Test A.

importance of the control of certain parameters in the fabrication of lightweight cellular concrete crash cushions. The compressive strength of the vermiculite concrete was increased to 71 psi and dimension B (Fig. 4) was increased to 2 in. The 24-1414 welded wire fabric was placed in the top and bottom of this barrier to eliminate the tendency of some portions of the barrier to scatter on impact. Because of these differences, the barrier was significantly stiffer than the previous barrier tested and a deceleration level of 10.3 g was observed. This corresponds to an average stopping force of approximately 33,000 lb. Overhead sequence photographs of this test are shown in Figure 8.

Based on the results of the first two tests, a third barrier (Fig. 5) was designed and tested that incorporated estimated stopping forces varying from 13,000 to 33,000 lb. The first 12 ft of barrier, with a predicted stopping force between 13,000 and 20,000 lb, would result in the deceleration of a 2,000-lb vehicle traveling 60 mph at a deceleration level slightly less than 10 g. The next 12 ft of the barrier, with 6 ft at a predicted 25,000 lb stopping force and 6 ft at 33,000 lb, would provide the necessary additional stopping force to decelerate a vehicle traveling 60 mph and weighing as much as 4,500 lb. This barrier was tested with a 4,560-lb vehicle traveling 63.6 mph, impacting head-on (Fig. 9). The estimated crushing force levels from photographic data show that the predicted stopping forces were fairly accurate. The vehicle was stopped in 21.4 ft at an average deceleration of 6.3 g, which means an average stopping force of 28,700 lb.

The final test, which was included for comparison purposes, was of a vehicle weighing 3,270 lb impacting a rigid wall at 53 mph. The average deceleration was 25 g and the stopping distance of the vehicle's center of gravity was 3.82 ft. The total vehicle residual crush was 3.25 ft.

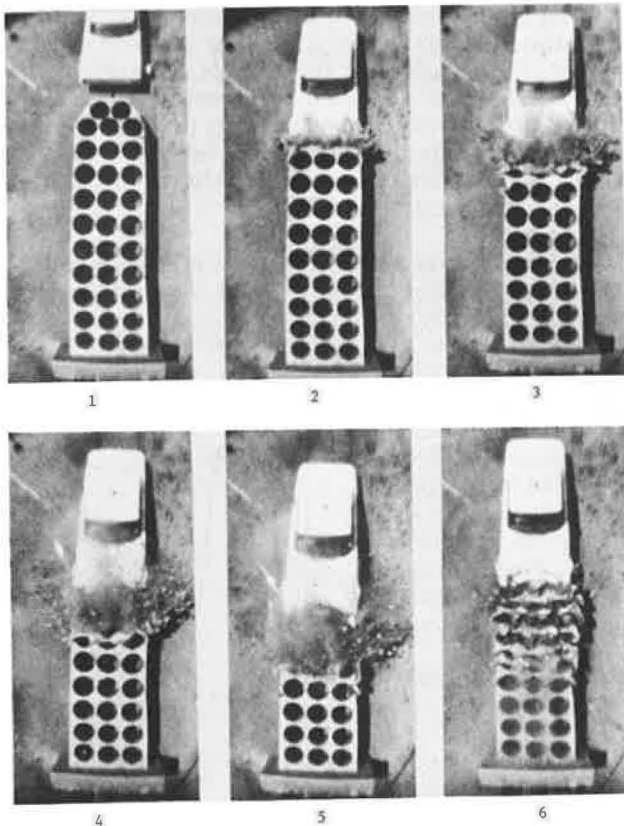


Figure 8. Overhead sequence photographs of Test B.

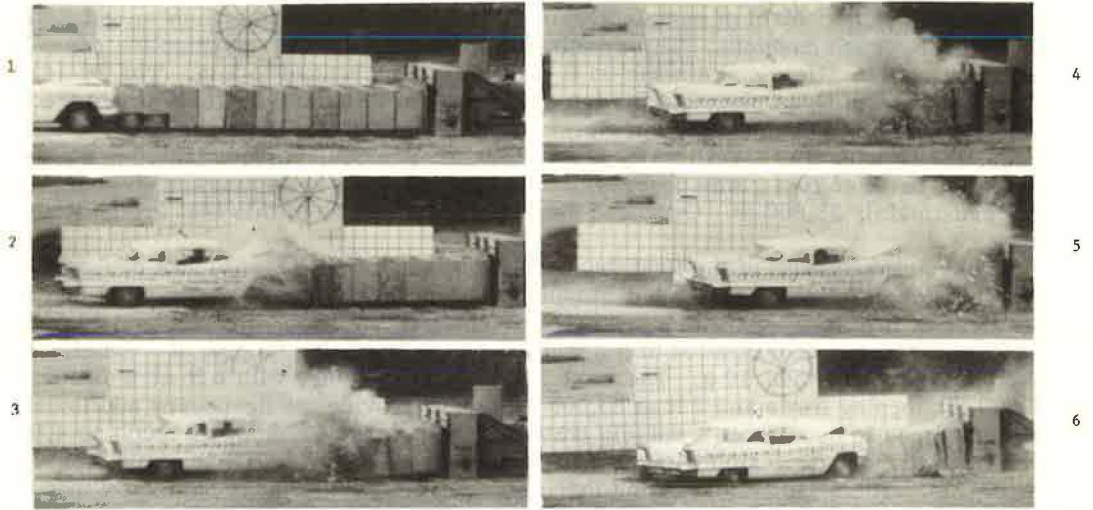


Figure 9. Sequential photographs of Test C.

A comparison of the severity of these crashes is given in Table 2 by the attenuation index. The maximum and average decelerations that would have been experienced by each vehicle had it struck a rigid barrier (for example, Test D) are calculated using accepted theory (2). The attenuation index is the ratio of the test maximum or average deceleration divided by the rigid barrier maximum or average deceleration respectively. The theory is an empirical generalization for all types of vehicles based on the particular vehicles tested by Emori, and could not be expected to give accurate decelerations for each vehicle tested. If the theory had accurately predicted the test decelerations, the attenuation index shown for this test would have been 1.0. The attenuation indexes for the three lightweight cellular concrete crash cushion tests show that the impact is approximately one-fourth to one-third as severe as it would have been had the vehicle struck a rigid barrier.

In Text A, only superficial sheet metal damage was sustained by the vehicle. The radiator was not moved with respect to the frame of the vehicle during the impact. In Test B, considerably more sheet metal damage was done to the vehicle and the radiator was moved back far enough to encounter the fan blades. However, the vehicle was driven away from the scene of the crash after the fan belt had been removed. In Test C, again only superficial sheet metal and some bumper damage was sustained. Test D (the immovable wall) resulted in the total and irreparable destruction of the vehicle.

Another way to demonstrate the differences between encountering a rigid obstacle and colliding with a crash cushion can be seen in Figure 10. Here the deceleration vs. time curves are given for the rigid wall test and for the last concrete crash cushion test. The crash cushion acts

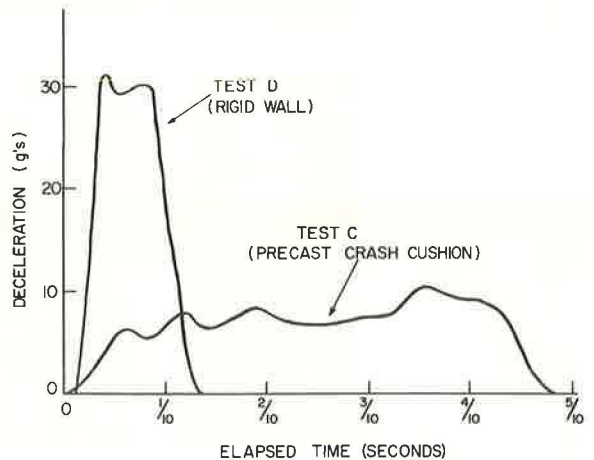


Figure 10. Comparison of decelerations.

to distribute the deceleration of the vehicle over a period of time that is approximately 5 times as great as that required to stop the vehicle when it encounters a rigid obstacle. The result is the significant lowering of the deceleration level indicated by Figure 10.

CONCLUSION

The lightweight cellular concrete crash cushion has been shown to be extremely effective in decelerating a vehicle during a head-on crash. Although side-angle hits have not been conducted, it is expected that further testing will show the acceptability for this collision condition also. This estimate is based on the acceptable reaction of the Modular crash cushion (3) composed of 55-gallon steel barrels, which functions in a very similar way. All tests show deceleration levels within the tolerance limits of restrained humans. The lightweight cellular concrete crash cushion can be installed by one of two methods by semi-skilled laborers. The formwork can be placed in the field, and a local vermiculite applicator can supply the necessary concrete; or the precast modular construction method can be used. The estimate of cast-in-place construction cost, including all materials and labor, is \$800 per installation. Using the modular construction technique, considerable savings should be realized by mass production.

Close quality control should be exercised on the geometry of the attenuator and on the vermiculite concrete. Control of batch proportions and unit weight will give predictable crushing strengths. Replacement of segments of the crash cushion can easily be accomplished after a collision. For a cast-in-place cushion, the crushed material can be removed, that portion of the barrier re-formed, and fresh vermiculite placed in the necessary areas. Fast-setting cement will alleviate the problem of curing time. For the precast cushions, the three-tube modules weigh approximately 250 lb, and could therefore be handled easily by four men. The modules that have been crushed during a collision can be unbolted, removed, and new modules slipped into place. This refurbishment could be accomplished during a low-density traffic period.

REFERENCES

1. Shoemaker, Norris E. Research and Design of an Impact Absorbing Barrier for Fixed Highway Objects. CAL Report No. VJ-2501-V-1, Cornell Aeronautical Laboratories, Buffalo, June 1968.
2. Emori, Richard I. Analytical Approach to Automobile Collisions. SAE Paper 680016, Engineering Congress, Detroit, Jan. 8, 1968.
3. Hirsch, T. J., and Ivey, Don L. Vehicle Impact Attenuation by Modular Crash Cushion. Research Rept. No. 146-1, Texas Transportation Institute, Jan. 1969.

Effect of Vehicle Collision With Aluminum Roadside Sign Structures Mounted on Frangible Bases

J. E. MARTINEZ, T. J. HIRSCH, YUCE BASKURT, and J. J. JUMPER,
Texas Transportation Institute, Texas A&M University

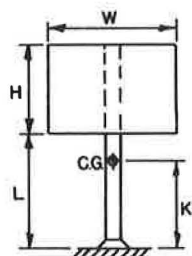
Roadside sign structures are usually located adjacent to a traffic lane and because of their location give rise to a safety hazard. Numerous collisions with these structures have been reported and in many instances serious injury or fatalities have occurred.

This paper presents the results of the mathematical simulation of vehicle collision with single and dual support aluminum roadside sign structures mounted on frangible bases. The study was performed with the aid of a mathematical model verified by a full-scale crash test and analyzed sign and sign support configurations that are typical of roadside sign structures proposed by the state of Maine. The equations of motion predicting the response of the system were solved numerically and a computer was used to obtain the results. Some findings of the study reveal that low-speed collisions (15-20 mph) normally cause the support to hit the windshield area of the vehicle; medium-speed collisions (30-45 mph) with the single support structure cause the support to strike the top or trunk area of the vehicle; and medium- and high-speed collisions with the dual support structure cause the post to clear the vehicle.

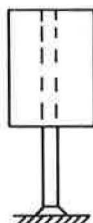
●AN EFFICIENT modern highway requires having roadway signs that relay information to the motorist in a clear and concise manner, and current highway design concepts for multilane facilities have resulted in the installation of sign supports near the edge of the traffic lane. Because of their location, these signs constitute a safety hazard, and collisions with these signs have caused fatalities.

An obvious solution to the problem is relocation of the support. This approach is usually not feasible, and the engineer must resort to other means to alleviate the dilemma. A design that has already shown considerable merit is the slip base type breakaway support that, upon impact, disengages the post from the foundation. This generally accepted design limits impact forces, but regard must be given to the possibility that the structure may fall on the vehicle and create a hazardous situation for the occupants.

The purpose of this investigation was to evaluate the crash-dynamic behavior of various aluminum sign structure configurations mounted on frangible bases having different impact characteristics. The base force-deformation behavior was obtained from laboratory tests performed by the Texas Transportation Institute, and the results used in the study are presented in the Appendix. The dynamic response of the vehicle and the structure was obtained with the aid of a mathematical model. Typical results are presented in Tables 3 through 10 in the Appendix.

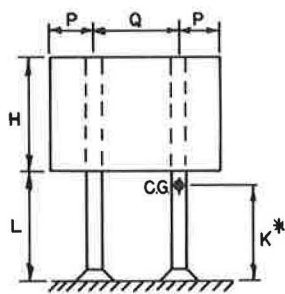


SIGN IA

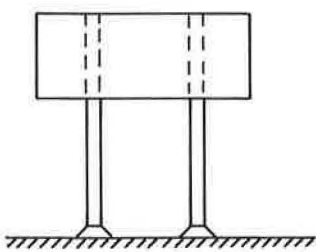


SIGN IB

SIGN	IA	IB
W (FT.)	6.0	4.0
H (FT.)	5.0	10.0
L (FT.)	7.0	6.0
WEIGHT (LBS.)	93.2	124.0



SIGN IC



SIGN ID

SIGN	IC	ID
P (FT.)	2.0	2.5
Q (FT.)	6.0	8.0
H (FT.)	9.0	6.0
L (FT.)	7.0	7.0
WEIGHT (LBS.)	111.6	93.0

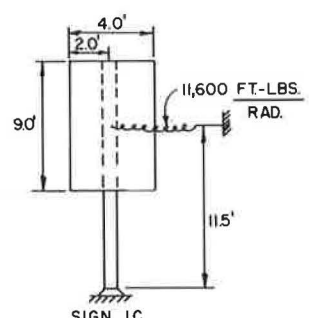
*FOR IDEALIZED SIGN (FIG.2)

Figure 1. Sign configurations used in study.

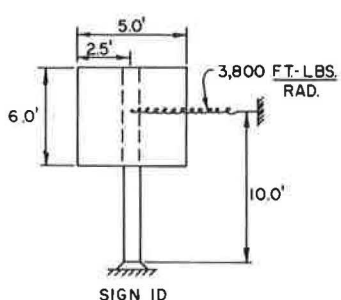
DESCRIPTION OF SIGN STRUCTURE

The aluminum signs and sign support configurations evaluated in this study are typical of roadside sign structures proposed by the state of Maine. These structures are shown in Figures 1 and 2. The complete post and sign description is given in Table 2 in the Appendix.

In the mathematical simulation it was assumed that the frangible bases deform by the amounts indicated in Figures 3 through 6. These deformations were obtained from accelerometer test data and represent the distance the impacting ram used in the base fracture test moved after initial contact with the base. This force-deformation ideal-



SIGN IC



SIGN ID

Figure 2. Idealizations of signs 1C and 1D.

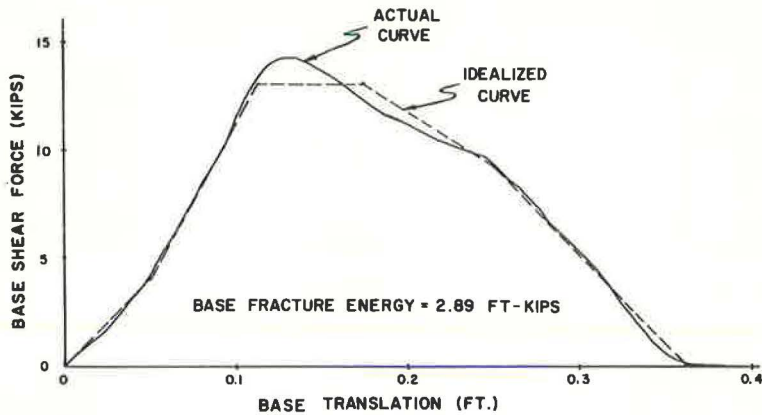


Figure 3. Base fracture energy curve for $6 \times \frac{3}{16}$ -in. post.

ization makes the peak forces encountered in the larger bases quite sizeable since the energy for all bases must be dissipated for a relatively small value of base deformation. The idealized curves also shown in Figures 3 through 6 represent the same base fracture energy as the experimental curves and were necessary to obtain the input to the computer coding, which assumes a piecewise linear variation of base shear force.

MATHEMATICAL SIMULATION

Two mathematical models were employed in the study. The model that yields the dynamic response of the single support structure assumes four degrees of freedom and is basically a planar version of the three-dimensional model that was employed in the analysis of luminaire support structures (1). This more recent model was coded in order to reduce the computer time associated with the solution of a problem. A Runge-Kutta numerical integration scheme (2) has also been added, making the program more efficient.

The model used to predict the behavior of the dual support structure assumes two degrees of freedom and idealizes the structure as being hinged at the center of the sign

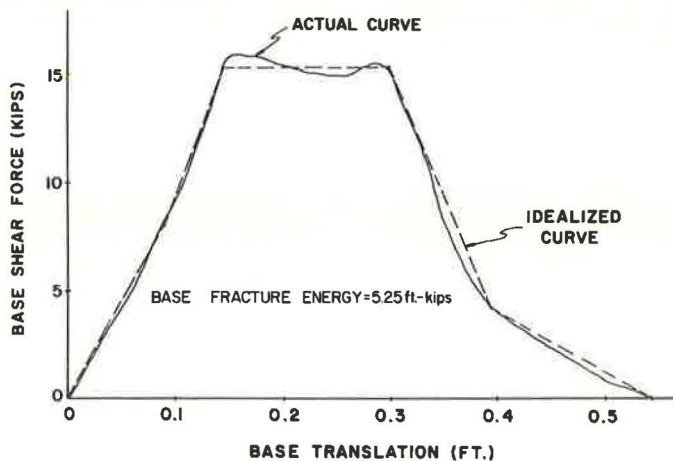


Figure 4. Base fracture energy curve for $8 \times \frac{1}{4}$ -in. post.

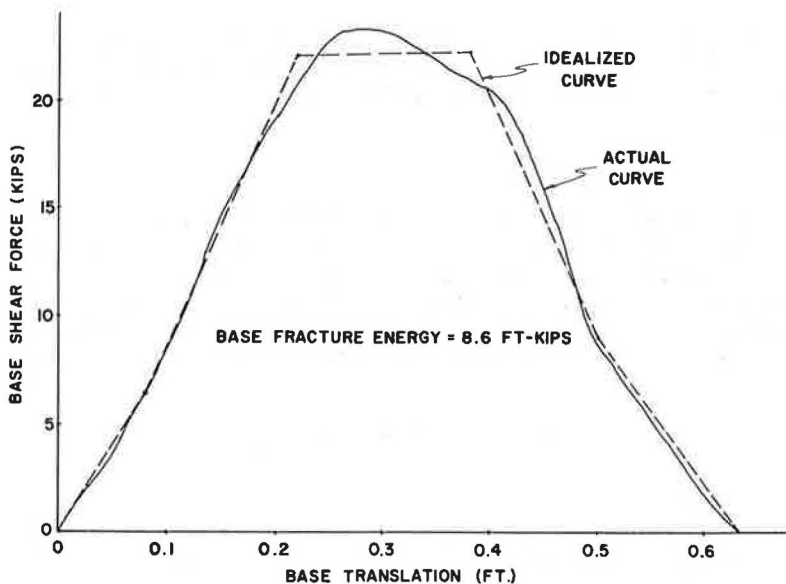


Figure 5. Base fracture energy curve for $10 \times \frac{1}{4}$ in. post.

and capable of having only a rotation about this point. The effects of the sign and of the support that is not impacted are lumped into a torsional spring constant, as shown in Figure 2.

The vehicle is represented as a single-degree-of-freedom spring-mass system having a spring of variable stiffness. The rigid mass and its velocity simulate the momentum

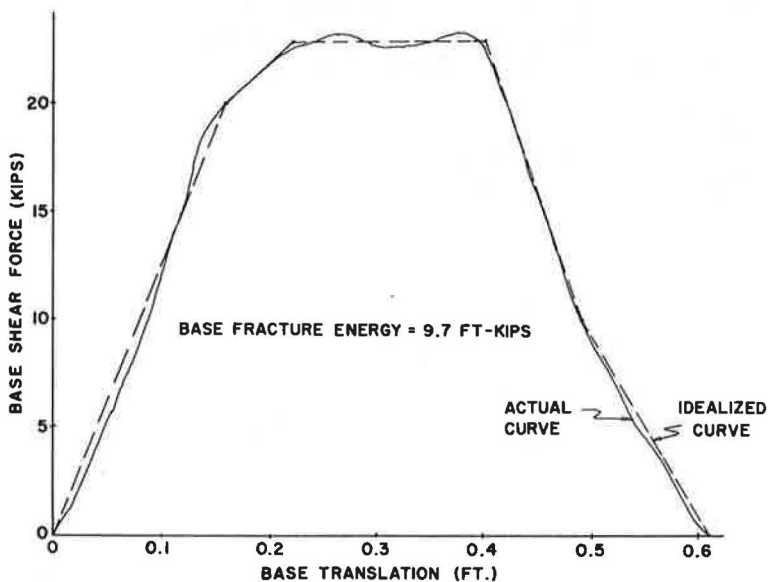


Figure 6. Base fracture energy curve for $12 \times \frac{1}{4}$ in. post.

of the vehicle and the energy absorbed is determined from the spring force-deformation relationship. In the study it was assumed that the spring constant was a function of the vehicle weight. The collisions were considered to take place for a vehicle approach angle of zero.

Verification of Mathematical Model

To verify the mathematical models, a full-scale crash test was performed at the Texas Transportation Institute Research Annex. The test employed a 1959 Ford sedan weighing 3,550 lb and sign 1A. The impact velocity was 29 mph.

Table 1 and Figure 7 present a comparison of model and crash test results and indicate good agreement. It is anticipated that the model will predict results very satisfactorily for most cases where the peak force encountered in fracturing the base is not extremely large.

DISCUSSION OF RESULTS

Single Support Structures

The study revealed that for impacting velocities up to 45 mph, the single support structure does not clear the vehicle. Sign 1B, being taller and having a higher mass-center position than sign 1A, has a greater tendency to clear the vehicle and will probably do so at the higher velocities. Figure 8 shows the response of sign 1B when it is subjected to a 45-mph collision. Collisions by the lightweight (2,500-lb) vehicles traveling at slow speeds (15 mph or less) may be considered hazardous as they cause the support structure to strike the windshield area of the vehicle in a majority of the cases. This is because at the slower speeds the post has a greater tendency to translate and ride the front of the vehicle before falling on it. The effect is more pronounced for collisions with the supports mounted on bases having a high base fracture energy.

The results further revealed that a lightweight vehicle traveling at speeds below 15 mph may be stopped when it collides with supports mounted on bases having fracture energies of 10 ft-kips or greater. This large change in velocity may have a severe effect on the vehicle occupants, and such collisions could be interpreted as hazardous.

Collisions that cause the signpost to strike the top of the vehicle will normally not be hazardous unless the structure is quite massive or the contact is made near the windshield area. If contact is initially made in the windshield area, then it is conceivable that, depending on the rotation of the post, a secondary impact with the hood or windshield by some other point on the post could occur.

Dual Support Structures

The results of the study of dual support structures disclose that, for the cases investigated, only the slow-moving vehicle encounters a secondary collision with the post.

TABLE 1
COMPARISON OF MODEL AND CRASH TEST RESULTS

Test	Initial Velocity (mph)	Change in Velocity (mph)	Post-Vehicle Contact Time (sec)	Average Vehicle Deceleration (g)	Remarks
Full-scale crash	29.0	2.7	0.084	1.47	Signpost rotates 105 deg and hits top of vehicle 10.75 ft from front bumper. Total time of event is 0.338 sec.
Mathematical model	29.0	2.5	0.084	1.33	Signpost rotates 105 deg and hits top of vehicle 10.25 ft from front bumper. Total time of event is 0.318 sec.

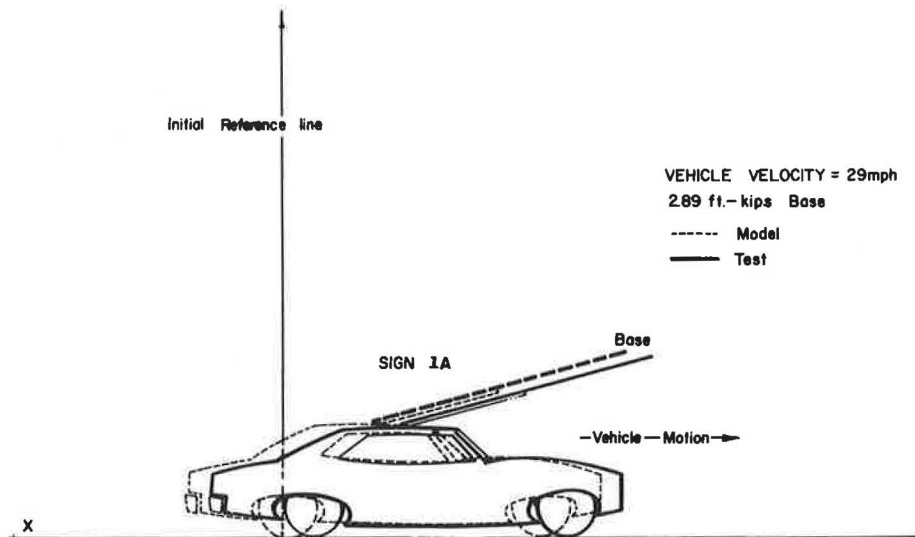


Figure 7. Comparison of model and crash test results, sign 1A.

This secondary collision occurs in the area of the windshield of the vehicle and may be interpreted as hazardous. The deceleration rates and velocity changes at these slow speeds are less than those obtained for the single support structures impacted at the same velocity. This is due to the dual support structure idealization and the high position of the assumed center of rotation.

Collisions at the higher vehicle velocities cause the post to clear the vehicle. This is due to the large angular velocity that is acquired by the relatively light support as a result of the vehicular impact. The response of sign 1C following impact by a medium-sized vehicle at various velocities is shown in Figure 9.

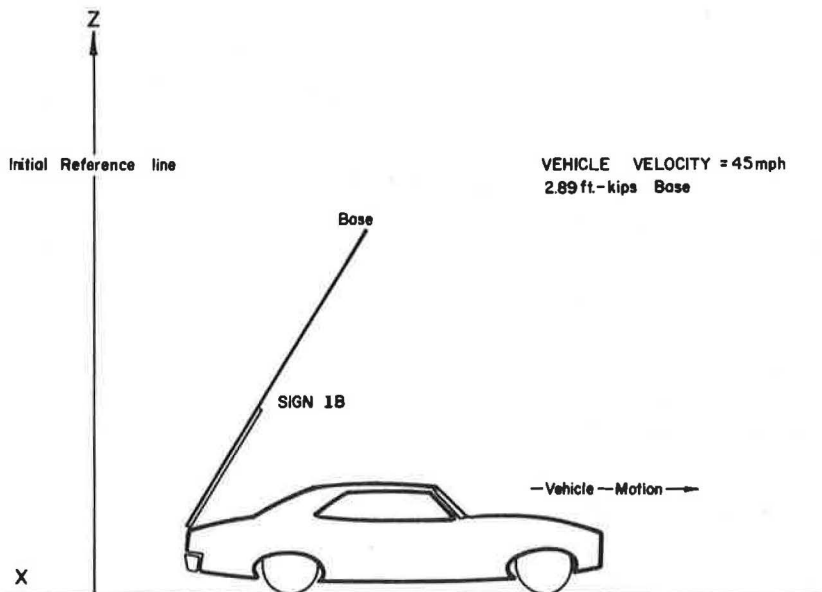


Figure 8. Typical impact response of sign 1B.

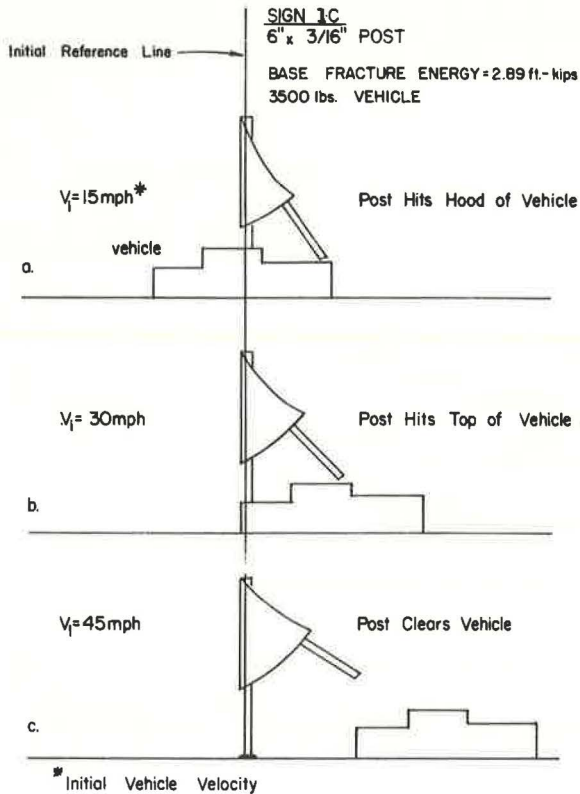


Figure 9. Typical impact response of sign 1C.

experienced when similar collisions involve the sign employing the single support. This can be partially attributed to the different sign geometric and inertia properties and the constraints imposed on the idealized structure. They produce the effect of causing the single support to stay in longer contact with the vehicle, thus accounting for the larger velocity changes.

GENERAL CONCLUSIONS

The general conclusions stated here are based on the cases investigated and a criterion that uses a vehicular velocity change of 11 mph as one that causes passenger injury (3).

In single support structures, the following conclusions may be stated:

1. Collisions by vehicles traveling up to 45 mph cause the supports investigated to strike the vehicle.
2. Collisions of lightweight vehicles traveling at speeds of approximately 15 mph may cause a hazardous condition (one that could cause passenger injury) when they impact the large-diameter support posts. This is based on vehicular velocity changes of approximately 11 mph.
3. Medium- and high-speed collisions will cause the support to strike the top or trunk areas of the vehicle. These cases are not usually hazardous.

In dual support structures, the following conclusions may be reached:

1. For the cases investigated, velocity changes remain below the criteria established for a hazardous condition.

Comparison

The results given in the tables in the Appendix show that the impact behavior of signs 1A and 1B is very similar. The higher center of mass of sign 1A gives it more of a tendency to rotate and, as a result, the rotation angle of the structure is greater when it rotates and strikes the vehicle. In general, it can be said that lowering of the center of mass of the structure will give the support more of a tendency to translate and will increase the vehicular change in velocity.

Signs 1C and 1D behave in much the same manner. The stiffer torsional spring assumed for sign 1C gives the structure a greater rotational stiffness and its effect becomes more pronounced for collisions of light vehicles with supports requiring the larger base fracture energies. In the case of a heavier vehicle impacting at a low velocity, the stiffer torsional spring of sign 1C causes the support to encounter a secondary collision in the hood or windshield area, whereas sign 1D has its support strike the top of the vehicle.

A comparison of the single and dual support structures indicates that greater vehicular velocity changes and deceleration rates will be exper-

2. Low-speed collisions (15-20 mph) will normally give rise to a secondary collision in the vicinity of the hood or windshield area. These collisions are not necessarily hazardous, however, as the post will not come through the windshield after the secondary collision takes place.

3. Medium- and high-speed collisions cause the post to clear the vehicle and the vehicular velocity changes remain within tolerable limits.

It should be emphasized that the assumption of the post and sign remaining fastened together during impact has been made. If the connections are not rigid enough, it is possible for the post and the sign to detach and possibly create an additional hazard as secondary collisions with both the post and sign would be encountered.

ACKNOWLEDGMENTS

This work was conducted under the Office of Research and Development, Structures and Applied Mechanics Division, Research Program on Structural Systems in Support of Highway Safety (4S Program). The opinions, findings, and conclusions expressed or implied in this report are those of the authors and not necessarily those of the U. S. Bureau of Public Roads.

REFERENCES

1. Martinez, J. E. An Investigation of the Impact Behavior of a Rigid Body. Doctoral dissertation, Department of Mechanical Engineering, Texas A&M University, Aug. 1967.
2. McCormick, J. M., and Salvadori, M. G. Numerical Methods in Fortran. Prentice-Hall, Inc., 1964, p. 242.
3. Patrick, L. M., et al. Knee, Chest, and Head Impact Loads. Proc. 11th Stapp Car Crash Conference, Anaheim, Calif., Oct. 10-11, 1967, p. 116.

Appendix

On the following pages, Table 2 gives the properties of the signposts, and Tables 3 through 10 give the results for the 4 signs with base fracture energies of 2.89 and 9.7 ft-kips.

TABLE 2. POST PROPERTIES FOR SIGNS USED IN STUDY

SIGN 1A

Post	6" x 3/16" ^c	8" x 1/4"	10" x 1/4"	12" x 1/4"
Post Height (ft)	12.0	12.0	12.0	12.0
Post Weight (lbs)	52.5	93.1	110.3	132.9
K ^a (ft)	8.2	7.7	7.6	7.4
Base Fracture Energy (ft-kip)	2.89	5.25	8.6	9.7

SIGN 1B

Post	6" x 3/16"	8" x 1/4"	10" x 1/4"	12" x 1/4"
Post Height (ft)	16.0	16.0	16.0	16.0
Post Weight (lbs)	70.0	124.1	147.1	177.2
K ^a (ft)	9.9	9.5	9.4	9.2
Base Fracture Energy (ft-kip)	2.89	5.25	8.6	9.7

SIGN 1C

Post	6" x 3/16"	8" x 1/4"	10" x 1/4"	12" x 1/4"
Post Height (ft)	16.0	16.0	16.0	16.0
Post Weight (lbs)	70.0	124.1	147.1	177.2
K ^b (ft)	11.5	11.5	11.5	11.5
Base Fracture Energy (ft-kip)	2.89	5.25	8.6	9.7

SIGN 1D

Post	6" x 3/16"	8" x 1/4"	10" x 1/4"	12" x 1/4"
Post Height (ft)	13.0	13.0	13.0	13.0
Post Weight (lbs)	56.9	101.0	119.5	144.0
K ^b (ft)	10.0	10.0	10.0	10.0
Base Fracture Energy (ft-kip)	2.89	5.25	8.6	9.7

^aFor center of gravity of post and sign (Fig. 1)

^bFor assumed center of rotation of idealized structure (Fig. 2)

^cPipe diameter and wall thickness, respectively

TABLE 3. RESULTS FOR SIGN 1A WITH BASE
FRACTURE ENERGY OF 2.89 FT-KIPS

Vehicle Weight (lbs)	Initial Vehicle Velocity (mph)	Change in Vehicle Velocity (mph)	Duration of Collision (sec)	Average Vehicle Deceleration (G's)	Remarks
2500	15	5.0	0.121	1.9	Post hits top of vehicle. L = 6.8 ft ^a
2500	30	2.9	0.091	1.4	Post hits top of vehicle. L = 10.9 ft
2500	45	2.3	0.080	1.3	Post hits top of vehicle. L = 12.6 ft
3500	15	3.4	0.124	1.3	Post hits top of vehicle. L = 7 ft
3500	30	2.5	0.084	1.3	Post hits top of vehicle. L = 10.4 ft
3500	45	2.1	0.069	1.4	Post hits top of vehicle. L = 12.2 ft
5000	15	1.9	0.098	0.9	Post hits top of vehicle. L = 7.3 ft
5000	30	1.3	0.072	0.8	Post hits top of vehicle. L = 10.5 ft
5000	45	1.1	0.066	0.7	Post hits top of vehicle. L = 12.4 ft

(a) L is the distance from front bumper of vehicle to point where support hits

TABLE 4. RESULTS FOR SIGN 1B WITH BASE
FRACTURE ENERGY OF 2.89 FT-KIPS

Vehicle Weight (lbs)	Initial Vehicle Velocity (mph)	Change in Vehicle Velocity (mph)	Duration of Collision (sec)	Average Vehicle Deceleration (G's)	Remarks
2500	15	5.5	0.129	1.9	Post hits top of vehicle. L = 9.8 ft ^a
2500	30	3.1	0.086	1.7	Post hits trunk area of vehicle.
2500	45	2.6	0.084	1.4	Post hits trunk area of vehicle.
3500	15	3.8	0.131	1.2	Post hits top of vehicle. L = 10.2 ft
3500	30	2.7	0.092	1.3	Post hits trunk area of vehicle.
3500	45	2.1	0.079	1.2	Post hits trunk area of vehicle.
5000	15	1.9	0.104	0.8	Post hits top of vehicle. L = 10.7 ft
5000	30	1.3	0.076	0.7	Post hits trunk area of vehicle.
5000	45	1.2	0.074	0.7	Post hits trunk area of vehicle.

(a) L is the distance from front bumper of vehicle to point where support hits

TABLE 5. RESULTS FOR SIGN 1C WITH BASE
FRACTURE ENERGY OF 2.89 FT-KIPS

Vehicle Weight (lbs)	Initial Vehicle Velocity (mph)	Change in Vehicle Velocity (mph)	Duration of Collision (sec)	Average Vehicle Deceleration (G's)	Remarks
2500	15	3.2	0.116	1.3	Post hits hood area of vehicle.
2500	30	2.0	0.075	1.2	Post hits windshield area of vehicle.
2500	45	2.3	0.075	1.4	Post has cleared the vehicle.
3500	15	2.3	0.120	0.9	Post hits hood area of vehicle.
3500	30	1.5	0.081	0.8	Post hits top of vehicle.
3500	45	1.7	0.071	1.1	Post has cleared the vehicle.
5000	15	1.6	0.094	0.8	Post hits hood area of vehicle.
5000	30	1.1	0.069	0.7	Post hits top of vehicle.
5000	45	1.2	0.067	0.8	Post has cleared the vehicle.

TABLE 6. RESULTS FOR SIGN 1D WITH BASE
FRACTURE ENERGY OF 2.89 FT-KIPS

Vehicle Weight (lbs)	Initial Vehicle Velocity (mph)	Change in Vehicle Velocity (mph)	Duration of Collision (sec)	Average Vehicle Deceleration (G's)	Remarks
2500	15	2.9	0.109	1.2	Post hits windshield area of vehicle.
2500	30	1.8	0.082	1.0	Post has cleared the vehicle.
2500	45	1.7	0.072	1.1	Post has cleared the vehicle.
3500	15	2.0	0.112	0.8	Post hits windshield area of vehicle.
3500	30	1.3	0.076	0.8	Post has cleared the vehicle.
3500	45	1.2	0.062	0.9	Post has cleared the vehicle.
5000	15	1.5	0.088	0.8	Post hits windshield area of vehicle.
5000	30	0.9	0.065	0.6	Post has cleared the vehicle.
5000	45	0.9	0.060	0.7	Post has cleared the vehicle.

TABLE 7. RESULTS FOR SIGN 1A WITH BASE
FRACTURE ENERGY OF 9.7 FT-KIPS

Vehicle Weight (lbs)	Initial Vehicle Velocity (mph)	Change in Vehicle Velocity (mph)	Duration of Collision (sec)	Average Vehicle Deceleration (G's)	Remarks
2500	15	9.2	0.153	2.7	Post hits windshield area of vehicle.
2500	30	7.0	0.057	5.6	Post hits windshield area of vehicle.
2500	45	6.8	0.044	7.0	Post hits top of vehicle. L = 7.0 ft ^a
3500	15	7.7	0.136	2.6	Post hits windshield area of vehicle.
3500	30	5.1	0.057	4.0	Post hits top of vehicle. L = 7.0 ft
3500	45	4.7	0.040	5.4	Post hits top of vehicle. L = 7.6 ft
5000	15	6.0	0.150	1.8	Post hits top of vehicle. L = 7.0 ft
5000	30	3.7	0.058	2.9	Post hits top of vehicle. L = 9.0 ft
5000	45	3.8	0.038	4.6	Post hits top of vehicle. L = 10.0 ft

(a) L is the distance from front bumper of vehicle to point where support hits

TABLE 8. RESULTS FOR SIGN 1B WITH BASE
FRACTURE ENERGY OF 9.7 FT-KIPS

Vehicle Weight (lbs)	Initial Vehicle Velocity (mph)	Change in Vehicle Velocity (mph)	Duration of Collision (sec)	Average Vehicle Deceleration (G's)	Remarks
2500	15	10.0	0.168	2.7	Post hits windshield area of vehicle.
2500	30	7.5	0.059	5.8	Post hits top of vehicle. L = 7.5 ft ^a
2500	45	7.4	0.046	7.4	Post hits top of vehicle. L = 8.5 ft
3500	15	8.5	0.162	2.4	Post hits windshield area of vehicle.
3500	30	5.8	0.058	4.5	Post hits top of vehicle. L = 11.0 ft
3500	45	5.3	0.042	5.8	Post hits top of vehicle. L = 12.0 ft
5000	15	6.2	0.157	1.8	Post hits top of vehicle. L = 8.0 ft
5000	30	4.2	0.065	2.9	Post hits trunk area of vehicle.
5000	45	4.1	0.040	4.7	Post hits trunk area of vehicle.

(a) L is the distance from front bumper of vehicle to point where support hits

TABLE 9. RESULTS FOR SIGN 1C WITH BASE
FRACTURE ENERGY OF 9.7 FT-KIPS

Vehicle Weight (lbs)	Initial Vehicle Velocity (mph)	Change in Vehicle Velocity (mph)	Duration of Collision (sec)	Average Vehicle Deceleration (G's)	Remarks
2500	15	9.5	0.152	2.5	Post hits hood area of vehicle.
2500	30	5.2	0.055	4.3	Post has cleared the vehicle.
2500	45	5.2	0.045	5.3	Post has cleared the vehicle.
3500	15	5.2	0.156	1.5	Post hits hood area of vehicle.
3500	30	3.8	0.053	3.3	Post has cleared the vehicle.
3500	45	3.8	0.040	4.3	Post has cleared the vehicle.
5000	15	3.6	0.144	1.1	Post hits windshield area of vehicle.
5000	30	2.7	0.060	2.0	Post has cleared the vehicle.
5000	45	2.7	0.040	3.1	Post has cleared the vehicle.

TABLE 10. RESULTS FOR SIGN 1D WITH BASE
FRACTURE ENERGY OF 9.7 FT-KIPS

Vehicle Weight (lbs)	Initial Vehicle Velocity (mph)	Change in Vehicle Velocity (mph)	Duration of Collision (sec)	Average Vehicle Deceleration (G's)	Remarks
2500	15	7.5	0.136	2.5	Post hits hood area of vehicle.
2500	30	5.2	0.052	4.5	Post has cleared the vehicle.
2500	45	3.6	0.041	4.0	Post has cleared the vehicle.
3500	15	5.1	0.123	1.9	Post hits hood area of vehicle.
3500	30	3.7	0.052	3.2	Post has cleared the vehicle.
3500	45	2.6	0.040	3.0	Post has cleared the vehicle.
5000	15	3.5	0.135	1.2	Post hits windshield area of vehicle.
5000	30	2.6	0.053	2.2	Post has cleared the vehicle.
5000	45	1.8	0.038	2.1	Post has cleared the vehicle.